Dynamical Climatology

Diurnal variation and cloud in a general circulation model

by

C.A.Wilson and J.F.B.Mitchell

DCTN 18 February 1985

Meteorological Office (Met. O. 20)
London Road
Bracknell
Berkshire RG12 2SZ

DYNAMICAL CLIMATOLOGY TECHNICAL NOTE NO. 18

DIURNAL VARIATION AND CLOUD IN A GENERAL CIRCULATION MODEL

by

C A Wilson and J F B Mitchell

This paper has been submitted for publication in the Quart. J. Roy. Met. Soc.

Met O 20 (Dynamical
Climatology Branch)
Meteorological Office
London Road
Bracknell
Berkshire, U.K. RG 12 2SZ

February 1985

Abstract

It is shown that changing the resolution of the diurnal cycle of cloud and radiative fluxes in an atmospheric general circulation model can affect the simulated climate. The effect on radiative forcing of using a temporal resolution which is unable to represent accurately the phase of diurnal variation in cloud is illustrated using a radiative convective version of the model. Similar results are found in the full model simulation for July, especially over land in the tropics. A detailed study of the changes over North Africa shows that the reduction in solar heating at the surface leads to a reduction in low level convergence and rainfall, and increased low cloud. The results indicate that cloud amounts need to be updated more frequently than 4 times a day if the model simulation is not to be degraded when the diurnal cycle is represented.

DIURNAL VARIATION AND CLOUD IN A GENERAL CIRCULATION MODEL

1. Introduction

A major topic in climate studies and modelling of climate and climate change is the role of clouds (eg NAS, 1982). Despite observational studies and sensitivity studies with climate models, it is still unclear whether clouds moderate or enhance the climate change caused by a perturbation of, say, atmospheric CO_2. The GARP report on climate and climate modelling (GARP, 1975) emphasised the importance of clouds in climate models and of representing their effects on different space and time scales correctly; especially important is the cloud radiation interaction. There are many possible feedbacks between cloud and the general circulation, and models must be capable of predicting cloud and representing these interactions realistically. Many climate models have excluded such feedbacks by using prescribed cloud amounts with fixed radiative properties and heights. Since most clouds are subgrid scale (either vertically or horizontally) the inclusion of clouds in models requires parametrization. Slingo (1980a) has discussed some of the difficulties in developing suitable schemes. A survey of cloud prediction schemes currently used in numerical models has recently been reported by Gilchrist (1983). In most schemes the cloud optical properties are fixed and cloud amounts and heights are diagnosed from the model convection schemes and/or relative humidity fields. Sensitivity studies of the influence of cloud cover on climate have been made with several models including such schemes (Crane and Barry, 1984).

This paper is concerned with the use of a cloud prediction scheme in an atmospheric general circulation model which includes the diurnal variation of solar radiation. A poor representation of the variations in cloud amounts through the day and their influence on the radiative fluxes can degrade the model's performance and could lead to large scale changes in the climate simulation. The errors can be decreased by diagnosing cloud and calculating radiative fluxes more frequently but this is usually very expensive in computer time. Our study used a cloud prediction scheme (Slingo 1980b), which allows fractional cover. Some models have a switch type scheme with only full or no cover possible at a grid point (Shukla and Sud, 1981; Hansen et al, 1983; Ghan et al, 1982). Such schemes are also likely to be sensitive to the resolution of the diurnal variation in cloud since it is the phase of this variation with respect to the imposed diurnal cycle in solar radiation that is important; the phase is dependent on the frequency of cloud prediction and radiation calculations.

Some of the climate models which have been used to study CO_2 induced climate change have omitted the diurnal cycle (Manabe and Wetherald, 1980; Washington and Meehl, 1983; Schlesinger, 1982). If the effects of clouds are to be properly included a diurnal cycle is necessary. Clouds affect the radiation balance in two ways: by reflecting a large part of the incoming solar radiation, and by enhancing the so called 'greenhouse' effect by increasing the downward infra-red flux and decreasing the outward radiance to space. These processes have opposing effects on the radiation balance. The solar contribution is only effective during the day so a realistic model should include diurnal variation of cloud and

radiation. Furthermore, it is necessary to include a diurnal cycle in order to investigate possible changes in surface climate such as maximum daily temperatures and the incidence of frosts.

2. The diurnal cycle and specification of cloud amounts

The estimation of radiative fluxes is computationally expensive so it is important to establish the maximum time between successive calculations (time step) which does not degrade the simulation significantly. With the diurnal cycle omitted and prescribed cloudiness, it is probably not necessary to calculate radiative heating rates more than once per day, since the most rapid changes in such fluxes (due to changes in atmospheric composition accompanying synoptic disturbances) are small. Again, if cloud amounts are prescribed, a fair representation of the diurnal cycle may be achieved by recalculating the radiative fluxes 4 times each day, provided the incoming solar radiation is averaged over the length of the time step (see for example Wilson and Mitchell, 1983). However, if cloud amounts are to be predicted from model variables, this technique will lead to errors in regions where there is a significant diurnal variation in cloudiness. In a model, cloud amounts and resulting radiative fluxes are diagnosed at the beginning of the time step and are held constant throughout. It is not possible to predict in advance what the 'average effective cloud amount' over that period will be. The nature of the errors resulting from inadequately resolving the diurnal cycle is best illustrated by the following idealised example. It is assumed that low cloud amount varies sinusoidally through the day, with total cover at 3.00 am and clear sky for several hours during the afternoon, as shown by

the smooth dashed line Figure 1a (the details are based on the modelled variation of low cloud over West Africa near 20°N in July shown in Figure 5a, referred to later in the paper). Remembering that the models cloud cover must be diagnosed at the beginning of the period for which it is valid, the variation of cloud amount diagnosed at discrete intervals will lag behind that of cloud diagnosed continuously. When the cloud amounts are updated at 2 hourly intervals, there is an overestimate of cloud amount in the morning, and an underestimate in the evening (Figure 1a, solid line) both of which become more pronounced when the interval is increased to 6 hours (chain dotted line). The daily averaged cloud amounts are 47% and 43% for 2 hourly and 6 hourly values respectively whereas the continuously diagnosed mean is 48%.

The change in radiative heating at the surface resulting from the lag in cloud variation shown in Figure 1a has been calculated using a one dimensional model based on the radiative, convective and surface parametrizations used in the Meteorological Office 5-layer general circulation model (Corby et al, 1977; Slingo, 1982). (The atmospheric profile and surface conditions were again based on the model results at 20°N over West Africa in July). Medium, high and convective cloud amounts were set to zero. The low cloud amounts and the resulting radiative fluxes are diagnosed at the beginning of each timestep. A mean cosine of zenith angle is computed over the interval to obtain an accurate estimate of incoming solar radiation. Increasing the time step from 2 to 6 hours decreased the downward solar flux at the surface from 281 Wm^{-2} to 233 Wm^{-2}, despite the decrease in daily averaged cloud. This is because the cloud cover is greater during the late morning in the integration with the

longer time step when incoming solar radiation is large, producing a large decrease in surface heating (Figure 1b). Although less cloud is diagnosed with coarse resolution in the early part of the night, there is no compensation as the incoming solar flux is negligible.

There are also changes in the evolution of the net long wave heating of the surface (not shown). With a decrease in the frequency of calculating cloud amount, there is less long wave cooling from the surface during the day, due to increased cloud cover, and lower surface temperatures, which is almost entirely compensated by increased cooling at night, due to reduced cloud cover and higher surface temperatures.

Of course, the change in solar heating at the surface due to increasing the time step will depend on the assumed pattern of cloudiness. The effect will be reduced for a smaller diurnal range of cloud cover, and will be reversed if the diurnal cloudiness is a maximum in the early afternoon (as one might expect with convective cloud over land) rather than in the early morning. Hence it is not possible to say a priori whether or not degrading the temporal resolution of cloud and radiative processes will increase or decrease the surface heating or how this will modify the circulation. In order to investigate this further we have carried out a numerical experiment described in the following sections.

3. The model, its climatology, and the numerical experiment

a. The model

A detailed study has been made using the Meteorological Office 5-layer general circulation model originally developed by Corby et al (1977). It is a primitive equation model, using an energy conserving finite difference scheme with a 10 minute time step. It uses a σ co-ordinate system (σ = pressure/surface pressure), with the atmosphere divided into 5 layers of equal mass. The horizontal grid gives a quasi-uniform resolution over the sphere with a grid length of approximately 330 km.

An explicit boundary layer height is carried and used to control convection and surface exchanges. Supersaturation is removed by condensing excess moisture as rain, and the static stability is controlled using a penetrative convection scheme (as modified by Bolton (1983)). The surface fluxes of heat and moisture are dependent on the surface stability (stable or unstable) and type (sea or land and ice). The original model has been modified to include an interactive radiation scheme, soil moisture and snow variables, seasonal variation of sea surface temperatures, sea ice extentsand ozone (Slingo, 1982), and model generated cloud cover (Slingo, 1980b; Wilson and Mitchell, 1983).

The radiation scheme is similar to that of Manabe and Strickler (1964). Solar radiation is absorbed and scattered by atmospheric gases (ozone, carbon dioxide and water vapour), clouds and the earth's surface. Both the diurnal and seasonal variation of solar zenith angle are accounted for. The cosine of zenith angle is averaged over the interval between updating the radiative fluxes in order to obtain an accurate estimate of incoming solar radiation. The radiative properties of clouds are given in Table 1.

The cloud prediction scheme was originally devised by Slingo (1980a), based on observations from the GARP Atlantic Tropical Experiment. The cloud cover C is a quadratic function of the model's relative humidity R, and a threshold humidity R_C.

$$C = (R - R_C)^2 / (100 - R_C)^2 \qquad R > R_C$$
$$C = 0 \qquad R \leq R_C$$

Up to 3 layers of cloud are permitted (high, medium and low); R_C = 70 for high cloud and 90 for medium and low cloud. Low cloud amount is also a function of the lapse rate in the lowest model layers, with the intention of modelling marine stratocumulus sheets which form under the lower tropospheric inversion on the eastern side of the subtropical anticyclones. A model inversion is defined by a potential temperature lapse rate $\Delta\theta/\Delta P$ between the two lowest model layers less than -0.07 Kmb^{-1}. In this case, low cloud cover C_L is given by

$$C_L = -16.67 \frac{\Delta\theta}{\Delta P} - 1.167 + \left(\frac{R-R_C}{100-R_C} \right)^2 \qquad R \geq R_C$$

$$C_L = -16.67 \frac{\Delta\theta}{\Delta P} - 1.167 - \left(\frac{R_C-R}{2R_C} \right) \qquad R < R_C$$

subject to the restriction $0 \leq C_L \leq 1$. A further constraint, that there should be a positive flux of sensible heat from the surface, was added to prevent the simulation of unrealistic amounts of low cloud under the polar night inversion. The contribution from the lapse rate term is generally negligible except on the eastern side of the subtropical oceans. Convective cloud cover is proportional to the maximum vertical mass flux computed by the model's convection scheme. Layer clouds are randomly overlapped in the vertical and not allowed to overlap convective cloud. The relative humidity used to determine each cloud type, and the level of the cloud top are determined according to table 2. In each case, the level with the higher relative humidity is used to determine the cloud amount and cloud top height. The radiative properties of the model clouds are again as given in Table 1.

b. The model's climatology

Aspects of the model climatology (using prescribed zonal cloudiness) have been presented by Slingo (1982) and Mitchell (1983). The model produces a mostly satisfactory simulation of the general circulation throughout the year, the main shortcomings being the over and underestimation of the depth of the mid latitude winter surface pressure troughs in the northern and southern hemisphere respectively, and excessive precipitation over the continents. In particular, the intertropical convergence zone over North Africa moves too far north into the Sahara in July. When the cloud prediction scheme is used, the simulated geographical distribution of cloud in January (Slingo, 1980b) and July (Figure 2) captures the

main features of the observed cloud distribution. The most noticeable shortcomings in the model cloud distribution are excessive medium and high cloud amounts over mountains, a failure to position high cloud correctly over the ITCZ, and greater than observed convective cloud over certain arid regions. These anomalies are generally associated with deficiencies in the moisture distribution in the model which are also evident when prescribed cloud amounts are used; in other words, they do not arise directly from deficiencies in the cloud prediction scheme. The July simulation is otherwise generally similar to that described by Mitchell (1983), except that there is significantly less precipitation over south East Asia, and more over North Africa and the Middle East.

The sensitivity of the model to changes in formulation should be most easily discerned in summer when the model's variability is least. Diurnal effects are likely to be most pronounced over land in latitudes where the daily amplitude of solar heating is greatest. Hence, in this paper we have concentrated on changes in the simulated climate over North Africa in June and July. It is appropriate therefore to consider the model climatology for this region in more detail.

The observed summer rainfall over North Africa is associated with the convergence zone near 10°N between moist southwesterly flow from the equatorial Atlantic, and drier air from the Sahara or North East Atlantic. Strong solar heating of the surface warms the atmosphere and produces a surface pressure trough near 20°N. Air at

low levels converges in the trough and is forced to ascend, releasing conditional instability. Air from the south is sufficiently moist to produce deep convection and rain, whereas air from the North is relatively dry; hence, in the North convection is shallow and in addition, is restricted to below about 600 mbs by subsidence from higher levels. In the south, convergence and precipitation are enhanced by the passage of squall lines and easterly waves (Burpee, 1977).

The incoming solar radiation at the top of the atmosphere has a local maximum near 40°N in July. The distribution of solar heating at the surface is modified by cloud, which in the model gives a minimum near 15°N, with much stronger heating to the North (Figure 3a). This produces a surface trough near 22°N, with strong low level convergence on the southern flank between Saharan air from the north and east, and moister air from the west or south west (Figure 3b). Along the simulated convergence zone is a band of intense precipitation (Figure 3c). Hence most of the features of the observed circulation are reproduced by the model. However, the main band of precipitation extends too far north, particularly over East Africa where the modelled subsidence aloft (not shown) is weak. It should also be noted that the model does not resolve squall lines, and the horizontal grid may be too coarse to resolve easterly waves accurately (for discussion of this see for example Krishnamurti et al, (1979), Gilchrist et al (1982)). Nevertheless, in both the observations and the simulation, one of the main factors promoting rainfall is convergence induced by solar heating at the surface.

The diurnal behaviour in the July integration is illustrated by the evolution through the day of a selection of near surface variables in and around the band of rain and cloud over North Africa (Figure 3c,d). The variation at A, to the north, B on the edge and C in the centre of the rainband, composited over a 10 day period, is shown by the solid lines in Figures 4, 5 and 6 respectively.

To the north of the rain band (Figure 4), there is no low cloud, convective cloud increases to a maximum during the early afternoon and dissipates overnight, and the diurnal range of surface temperature is 30 K. At the edge and in the centre of the rain band, (Figures 5 and 6 respectively) low cloud amounts increase to give almost complete cover overnight, and dissipate completely during the late morning, whereas convective cover is greatest in the early afternoon. The surface temperature ranges are 13 K and 5 K respectively. A broad comparison with observed data (for example Meteorological Office 1983) indicates that the diurnal range of temperature is realistic, but that the model relative humidities are probably too high. A more precise validation is not justified, since the observed rainband is centred near 10°N, well south of that in the model over most of Africa (Fig 3c), which adds to the difficulties of comparing observed data from individual stations with information from model grid boxes (see for example, Reed 1984, Wilson and Mitchell, 1984). Published data on the observed variation of cloudiness are hard to obtain. However, Lobanova (1967), using observations made during the International Geophysical Year, showed

that for rainy areas of West Africa at least, all forms of stratiform cloud occur with maximum frequency at night (2200 to 0300) or during the morning (0400 to 0900). This provides no information on the amplitude but the phase of the variation of low cloud in Table 3 and Figures 5 and 6 is probably correct.

In the model, precipitation is heaviest between 1200 and 1800 hours local time, (for example Table 3) coinciding approximately with the maximum in convective cloud. Burpee (1977) analysed the diurnal variation of the frequency of observations of moderate to heavy precipitation over tropical North Africa, (June to September, 1966-1969) and found that the maximum was generally later, usually 1800 or 2100 GMT. Observations at stations in northern Nigeria show rain occurring most often during the evening and over night (Nigerian Meteorological Services, 1960). Satellite data from GATE, as analysed by McGarry and Reed (1978) suggest that the maximum in convective cloud cover occurs just after midnight. These studies indicate that the diurnal maximum in the simulated precipitation occurs earlier than observed.

c. The experiment

Two 50 day integrations have been carried out, starting from the same initial conditions for 12 June of the fourth year of a multi-annual simulation (Mitchell, 1983). The 30 days previous to this date were rerun with the model as described in section 3(a), but with prescribed cloud. The results presented here (unless otherwise

stated) are averaged over the final 30 days, corresponding to the last 30 days of July. In the control integration, the cloud amounts and radiative heating rates were calculated from the instantaneous model fields every 2 hours, and applied through the next 2 hours. In the anomaly integration, the interval was increased to 6 hours. (The reader is reminded that the cosine of the solar zenith angle is averaged over the appropriate time interval, so that the 24 hour average of the incoming solar radiation at the top of the atmosphere is the same in both integrations).

4. Results

a. Changes in solar heating and cloud amounts

Over the last 30 days of the experiment, there is a consistent increase of 0.03 in the mean cloud amount over land due to decreasing the frequency of updating the model cloud amounts (Figure 7, Table 4). The changes in medium, high and convective cloud amounts are small, (Table 4), and so have little effect on the surface flux. The expected reduction in solar flux at the surface due to the changes in mean low cloud amount can be estimated from the properties in Table 1. Assuming no atmospheric absorption between low cloud base and the ground, the solar flux at cloud top is deduced to be about 260 Wm^{-2}, and the reduction at the surface only $6Wm^{-2}$, compared with the 12 Wm^{-2} actually obtained (Table 4). There is also a small decrease

(about 3 Wm^{-2}) in the long wave cooling of the surface. Some of the largest changes in solar flux occur in low latitudes, notably over North Africa and South East Asia (Figure 8).

To understand these changes more clearly, we have made a detailed study over a large region (6°N to 36°N, 10°W to 35°E) comprising most of North Africa, during a 10 day period in the middle of July. Over this period, the limited area mean low cloud amount was increased from 0.20 to 0.25, and the solar flux at the surface was reduced by 26 Wm^{-2} (Table 5). Again the decrease in the solar flux is much larger than the 12 Wm^{-2} expected due to the increase in mean cloud amount alone, and the decrease in absorbed solar flux of 20 Wm^{-2} dominates the reduction of 5 Wm^{-2} in the cooling of the surface by long wave radiation.

The evolution of the low cloud amount and the solar heating at the surface through the day (averaged over the 10 day period, Figure 9)[1] is similar to that in the idealized example discussed earlier. The phase of the cloud variation in the integration with the longer time step lags behind that with the shorter time step. As a result, the maximum reduction in solar heating at the surface (89 Wm^{-2} or 16%) occurs between 0600 and 1200 GMT (Table 3), when the difference in low cloud amount is greatest, and the incoming solar radiation is strongest. The reduction in surface heating contributes to a reduction in convective activity during daylight hours, which is

---

1
+ The time is GMT. The difference in local noon (3 hours between the eastern and western boundaries) has been neglected in this analysis.

manifested by a decrease in convective cloud amount (Table 3). Although there are also changes in medium and high cloud, (Figure 9) the changes in low cloud are dominant over most of the region.

The reduction in surface heating lowers the surface temperature, the transfer of sensible heat from the surface (Figure 9) and hence the temperature of the lowest layer, particularly during the day. On the other hand, the changes in specific humidity are small (Figure 9), so relative humidity, and hence low cloud amounts are increased (Figures 5, 6, 9, Tables 4, 5) leading to a further reduction in solar heating at the surface. This result is consistent with Wetherald and Manabe (1981), who found that reduced surface heating led to an increase in low cloud in regions where the atmosphere is not inherently stable due to large scale descent.

We have shown that the reduction in surface heating accompanying the larger time step is due to the consequent lag in the phase of the cloud amount, and that this is reinforced by a positive feedback between surface heating and low cloud amounts. This conclusion is consistent with the result from another 10 day period (the first 10 days of the experiment) and also a different region (centred over land at 90°E). We now consider the geographical distribution of the changes over North Africa.

The phase lag in the variation of low cloud will lead to the biggest changes in solar flux where the reduction in low cloud through the day is largest and most rapid. Over most of the region,

low cloud is a maximum in the early hours of the morning, and is reduced to 10% of total cover or less by early afternoon (the variation at points A, B and C, and averaged over the area can be seen in Figures 4–6 and Figure 9 respectively), so, to a first approximation, the diurnal variation is most marked where daily mean low cloud cover is most extensive (Figure 3d). In the absence of other effects, we would expect the changes in surface solar flux to be negligible in the north of the region, largest in the band of low cloud (Fig 3d) and small in the south, in broad agreement with the simulated changes (Figure 10a). However, the maximum decreases in solar heating and increases in low cloud (Figure 10b) are displaced to the north of the cloud band. This is consistent with the most rapid variation in low cloud amount occurring there, north of the centre of the cloud band (for example, points B and C, Figures 5(a), 6(a)). The large changes in cloudiness may be initiated by the largest surface heating changes discussed above and amplified by the feedback between surface heating and low cloud. The poleward shift of the rain band (discussed in the following Section) may also contribute to the increase in low cloud so providing a further feedback to enhance the decreases in solar heating at the surface caused by the change in updating cloud amounts.

b. Changes in circulation and precipitation

There is a reduction in the global mean precipitation over land accompanying the weakening of the solar heating at the surface (Table 4). Regions of reduced precipitation coincide broadly with

areas of reduced surface heating, (Figures 8 and 11a), at least over land in the tropics. On closer examination of the differences over North Africa and South East Asia, it appears that the greatest diminution in solar heating occurs just to the north of the largest decreases in rainfall. The reduction in rainfall occurs even though cloud cover, and by implication, relative humidity increase. This is still true on a regional scale (Figure 11b). For example, there is generally an increase in cloud over Central America, North Africa and Southeast Asia, even though precipitation diminishes there. Again, we turn to the detailed changes over North Africa to understand the model's response more clearly.

The change in timestep (and increase in cloud cover) contribute to the reduction in net downward radiation at the top of the atmosphere (Table 5), particularly along the northern edge of the rainband (Figure 12). This reduction in the radiative heating of the atmospheric column and surface must in the longer term be balanced by dynamical changes. Charney (1975) proposed that a reduction in net radiation would be balanced by atmospheric warming due to increased subsidence, which in turn would lead to a reduction in precipitation. The results presented here appear to be consistent with this argument, since there is a weakening of convergence in the bottom level which indicates a decrease in ascent (Table 6). The net flux of moisture from the atmosphere to the surface diminishes over North Africa (precipitation minus evaporation is 0.39 mm/day or 27% lower, Table 5). Since the moisture content of the atmosphere changes little over the ten day period, this implies that there is also a

reduction in the amount of moisture and hence latent heat advected into the area. This change (about 11 Wm^{-2}), combined with the change in net radiative heating of the column and surface, is equivalent to 0.2 K/day cooling throughout the depth of the atmosphere.

Model simulations of the circulation over the tropical continents are known to be sensitive to factors other than changes in radiative heating. Walker and Rowntree (1977) demonstrated the influence of surface moisture on the circulation and precipitation over an idealised tropical continent, even when the radiative heating was unchanged. Here, there is a decrease in soil moisture along the rainband (typically 2 cm), and a slight enhancement to the north, but the area mean reduction in evaporation is little over a fifth of the change in precipitation, suggesting that changes in surface hydrology are of secondary importance. Cunnington and Rowntree (1984) found that the simulated precipitation over North Africa was substantially reduced when the atmosphere was initially prescribed as being dry rather than moist. However, the difference in the atmospheric moisture content over North Africa during the 10 day period from the present experiment is small (less than 1%). The dominant factor appears to be the change in the radiative heating of the atmospheric column and surface accompanied by the change in the release of latent heat, resulting from a reduction in the convergence of moisture into the region. These changes are now considered in more detail.

We have seen earlier that one of the main factors promoting rainfall is convergence induced by solar heating at the surface. Furthermore, reducing the frequency of updating cloud amounts produces a marked decrease in the solar flux at the surface near 20°N (Figure 10a) and reduces the southward extent of the region of strong heating (Figure 13a, compared with Figure 3a). This leads to a pronounced weakening of the main low-level convergence zone (Figure 13b, compare Figure 3b). Consequently, the model's rainband becomes substantially weaker (Figure 13c), and shifts slightly north, following poleward contraction of the area of strong heating. Accompanying this shift there is a local increase in low cloud (Figure 10b) which enhances the reduction in solar heating at the surface expected on reducing the frequency of updating cloud amounts alone.

Two important points emerge from the changes outlined above. First, the largest changes in precipitation (Figure 14) do not coincide with the largest changes in solar heating (Figure 10a) but are displaced to the south. This is consistent with the circulation in the control run, where most precipitation occurs on the southern fringe of the region of strong heating (Figures 3a, 3c). Thus, the changes in solar heating affect precipitation remotely through changes in circulation, rather than directly through changing the static stability near the surface, and hence the local convective rainfall. Second, precipitation decreases over the region, even though layer cloud and relative humidity increase. In the simulation rainfall in low latitudes is produced by convection which does not

require saturation of grid box variables to give precipitation. The decrease in precipitation is mainly in the convective amounts (see reduction in convection cloud amount, Figure 9), and so need not be accompanied by a decrease in relative humidity.

Although there is a weakening of the low-level convergence and hence precipitation in the region, the area covered by air converging at low levels, producing ascent, saturation and low cloud is not altered substantially (compare Figures 3b, 13b). Wetherald and Manabe (1980) found a decrease in precipitation accompanied by increased low cloud cover in a series of idealised experiments in which they changed the solar constant. Their model omitted diurnal variation, and used a moist convective adjustment. They found that upward motion in the upper troposphere became not only less intense, but also occurred over a broader region in the integrations with a lower solar constant, decreasing condensation and increasing the area mean humidity and cloudiness. Although it is not clear that the same mechanism contributes to the increase in low cloud it is of interest that in both studies a decrease in surface heating produces an increase in cloud cover at least in regions where the atmosphere is inherently unstable. Both here and in the GFDL experiments, the change in surface heating is amplified by changes in cloud cover. Hansen et al (1984) also report an increase in cloud cover in integrations in which the solar constant or atmospheric CO_2 concentrations were decreased, though they do not describe the processes responsible.

5. Concluding remarks

We have shown that the simulation of climate in a general circulation model will be degraded if the diurnal cycle is not resolved adequately. Although the arguments presented in the paper are largely derived from the changes over North Africa in a 10 day period, similar changes in cloudiness, solar heating of the surface and precipitation are evident in the mean July simulation throughout the tropics over land. Updating cloud amounts and solar fluxes a mere 4 times per day appears to be inadequate, and likely to degrade the model simulation, particularly over the tropical continents. The obvious solution is to update the radiative fluxes more frequently, but this may prove too costly in terms of computer time. One alternative is to store the calculated solar fluxes several times per day and to diagnose cloud amounts more frequently, updating solar fluxes approximately to allow for changes in the reflection and transmission, although this will require more computer storage. Over North Africa, it was found that reduced surface heating weakened both the convergence of air at low levels and the intensity of precipitation. These changes in surface heating were reinforced by an increase in low cloud. This result is consistent with those obtained elsewhere in experiments in which the solar constant was varied, although it is not clear that the same mechanisms were responsible for this positive feedback.

Although this paper has emphasised the role of the diurnal variation of cloud cover in climate models, the main conclusion is equally applicable to Numerical Weather Prediction (NWP) models. Many NWP models now include a full diurnal cycle to

provide for the evolution of surface temperatures, showers and so forth. These phenomena are profoundly influenced by the radiative heating of the surface, which in turn is highly dependent on cloud cover. Our results indicate that in order to simulate these diurnal effects realistically, the diurnal cycle of radiation and cloud must be resolved adequately.

Table 1. Cloud properties used in the radiation scheme

Cloud Type	Low	Medium	High	Convective
Thickness ($\Delta\sigma$; $\sigma=P/P^*$)	0.05	0.05	0.02	Variable
Reflectivity	0.7	0.6	0.2	0.7
Transmissivity	0.2	0.3	0.75	0.2
Absorptivity	0.1	0.1	0.05	0.1
Emissivity	1.0	1.0	0.5	1.0

Table 2.

Cloud Type	Layer of R.H. used (σ)	Cloud top (σ)	Remarks
High	0.3	0.3	Cloud top at σ = 0.2 if convective cloud top is at σ = 0.2.
	0.5	0.4	
Medium	0.5	0.5	Cloud top at 0.7 if polewards of 60° lat.
	0.7	0.6	
Low	0.7	0.7	If medium cloud top at σ = 0.7, uses R.H. at σ = 0.9, cloud top at σ = 0.8.
	0.9	0.8	Puts cloud top at σ = 0.9 if boundary layer top lower than σ = 0.9.

Note: (1) If R.H. at σ = 0.5 > RH at σ = 0.3, σ = 0.7, both high and medium cloud are derived from R.H. at σ = 0.5.

(2) If R.H. at σ = 0.7 > R.H. at σ = 0.5, 0.9, both medium and low cloud are derived from R.H. at σ = 0.7.

Table 3. Diurnal variation over North Africa. (Mean over 6°N to 36°N, 10°W to 35°E, land points only)

C = control, D = anomaly-control

Period (GMT)	Low cloud Amount		Convective Cloud Amount		Solar flux at Surface (Wm^{-2})		Precipitation (mm)		Net downward radiation at the top of the atmosphere (Wm^{-2})
	C	D	C	D	C	D	C	D	D
00–06	.33	−.02	.04	.00	33	0	0.66	−0.05	2
06–12	.27	.16	.08	−.04	573	−89	1.16	−0.21	−53
12–18	.07	.10	.23	−.06	421	−11	1.52	−0.26	−8
18–24	.13	−.03	.08	.06	3	0	0.53	0.02	3

TABLE 4. JULY GLOBAL MEAN CLOUD AMOUNTS, SOLAR FLUX REACHING THE SURFACE AND NET LONGWAVE RADIATION OUT OF SURFACE (LAND ONLY)

INTEGRATION	CONTROL	ANOMALY	DIFFERENCE
Timestep for updating cloud amounts (hours)	2	6	
Total cloud amount	0.501	0.524	0.023
Convective cloud amount	0.080	0.078	-0.002
Low cloud amount	0.302	0.333	0.031
Medium cloud amount	0.096	0.097	0.001
High cloud amount	0.147	0.153	0.006
Solar flux at the surface (Wm^{-2})	198	187	-12
Net solar flux absorbed at surface (Wm^{-2})	165	155	-10
Net long wave radiation at surface (Wm^{-2})	55.3	52.4	- 2.9
Total Precipitation (mm/day)	3.17	2.86	- 0.31

Table 5. Area means over North Africa (6°N to 36°N, 10°W to 35°E, land only) composited over 10 days

	CONTROL	ANOMALY	DIFFERENCE
Low cloud amount	0.20	0.25	0.05
Convective Cloud amount	0.11	0.10	-0.01
Solar flux reaching the surface (Wm^{-2})	258	232	-26
Net Solar flux absorbed at surface (Wm^{-2})	211	191	-20
Net upward long wave radiation at surface (Wm^{-2})	57	52	- 5
Net downward flux at the top of the atmosphere (Wm^{-2})	35	21	-14
Precipitation (mm/day)	3.87	3.38	-0.49
Evaporation (mm/day)	2.42	2.32	-0.10
Sensible heat (Wm^{-2})	85.2	73.8	-11.4

Table 6. Area mean divergence over North Africa (6°N to 36°N, 10°W to 35°E), sampled every 6 hours over a ten day period (10^{-5} sec^{-1})

σ-level	Control	Anomaly-Control
0.3	0.97	-0.36
0.5	0.20	0.01
0.7	0.15	0.25
0.9	-1.37	0.23

References

Bolton, J A 1981 The estimation of zonally averaged climatological cloud data for use in the 5 level model radiation scheme. Met O 20 Tech Note II/136. UK Meteorological Office, Bracknell, England.

Burpee, R W 1977 The influence of easterly waves on the patterns of precipitation in tropical northern Africa. In 'Lectures on Forecasting tropical Weather, including tropical cyclones, with particular relevance to Africa'. WMO, No 492, Geneva.

Charney J G 1975 Dynamics of deserts and droughts in the Sahel (Symon Memorial Lecture) Q.J.R. Meteorol. Soc. 101, 193-202.

Corby, G A, Gilchrist, A and Rowntree, P R 1977 United Kingdom Meteorological Office 5-level general circulation model. Methods in Computational Physics, Academic Press, New York, San Francisco and London. Vol 17, 67-110.

Crane R G and Barry R G	1984	The influence of clouds on climate with a focus on high latitude interactions. J. Climatol., 4, 71-93.
Cunnington W M and Rowntree P R	1984	The sensitivity of the Saharan region in a general circulation model. To be submitted to Q.J.R. Meteorol. Soc.
GARP	1975	The physical basis of climate and climate modelling. GARP Pub series No 16. ICSU/WMO 265 pp.
Ghan, S J, Lingaas, J W, Schlesinger, M E, Mobley, R L, Gates W L	1982	A documentation of the OSU two-level atmospheric circulation model. Climate Research Institute Report No. 35 Oregon State University, Corvallis, Oregon.
Gilchrist, A	1983	Report to WGNE on cloud radiation interaction WCRP. Research activities in atmospheric and oceanic modelling Report No. 5.
Gilchrist, A, Rowntree, P R and Shaw, D B	1982	Large scale numerical modelling Ch. 6 of 'The GARP Atlantic Tropical Experiment'. GARP Pub Series No. 25 ICSU/WMO 477 pp.

Hansen, J, Russell, G 1983
Rind, D, Stone, P,
Lacis, A, Lebedeff S,
Ruedy, R and Travis, L
Efficient three-dimensional global models for climate studies: models I and II. Mon. Wea. Rev. 111, p 609-662.

Hansen, J, Lacis, D, 1984
Rind, D, Russell, G,
Stone, P, Fung, I,
Lerner, J, and Ruedy, R
Climate Sensitivity Experiments with a three-dimensional model: Analysis of Feedback Mechanisms. 'Climate Processes and Climate Sensitivity' (Maurice Ewing Series, 5, eds. J E Hansen and T Takahshi). AGU Washington 368 pp.

Krishnamurti, T N, 1979
Hua La Pan,
Chia Bo Chang,
Ploshay, Jeff, Walker,
David, Oodally, A Wahed
Numerical Weather Prediction for GATE. Q.J.R. met. Soc. 105, 979-1010.

Lobanova, V Ja 1967
Climatic charts of cloudiness in northern hemisphere. January and July (period IGY and IGC).
Moscow, Navco-Issledovateliskij Institut Aeroklimatogii.

Manabe, S and Strickler, R F 1964 Thermal equilibrium of the atmosphere with convective adjustment. J Atmos. Sci., 21, 361-385.

Manabe, S and Wetherald, R T 1980 On the distribution of climate change resulting from an increase of CO_2 content of the atmosphere. J. Atmos. Sci., 37, 99-118.

Meteorological Office 1983 Met O 856d. Tables of temperature, relative humidity, precipitation and sunshine for the world. Part 4 Africa, the Atlantic Ocean south of 35°N and the Indian Ocean.

McGarry, Mary M and Reed, Richard J 1978 Diurnal Variations in Convective Activity and Precipitation during Phases II and II of GATE. Monthly Weath. Rev. 106 101-113.

Mitchell, J F B 1983 The seasonal response of a general circulation model to changes in CO_2 and sea temperatures. Q.J.R. Meteorol. Soc., 109, 113-152.

NAS 1982 Carbon Dioxide and Climate, – a second assessment, US National Academy Press, Washington DC, 72 pp

Nigerian Meteorological Service 1960 Diurnal variation of rainfall. Meteorological Note No. 9. Lagos.

Reed D N 1984 Model simulation of temperature and precipitation in a multi-annual integration of a general circulative model. Met O 20 Tech. Note II/197.

Schlesinger, M E 1982 Preliminary analysis of the climatic response to doubled CO_2 simulated by the OSU atmospheric GCM with a coupled swamp ocean. Climatic research institute. Oregon State University,

Shukla J and Sud Y 1981 Effect of cloud radiation feedback on the climate of a general circulation model. J. Atm. Sci, 38, 2337–2353.

Slingo, J M 1980a A cloud parametrisation scheme derived from GATE data for use with a numerical model. Q.J.R. Meteorol. Soc., 106, 747-770.

1980b Interactive cloud and radiation in the Meteorological Office general circulation model. Proceedings of workshop on 'radiation and cloud radiation interaction in numerical modelling', ECMWF, 15-17 October 1980.

Slingo, J M 1982 A study of the earth's radiation budget using a general circulation model. Q.J.R. Meteorol. Soc., 108, 379-405.

Washington, W M and Meehl, G A 1983 General circulation model experiments on the climatic effects due to a doubling and quadrupling of carbon dioxide concentration, J Geographical Res., 88, 6600-6610.

Wetherald, R T and Manabe, S 1980 Cloud Cover and Climate Sensitivity. J. Atmos. Sci, 37, 1485-1510.

Wilson, C A and Mitchell, J F B 1983 Interactive cloud in the 5 level model. Met O 20 Tech Note II/195. UK Meteorological Office, Bracknell, England.

Wilson, C A and Mitchell, J F B 1984 The 5-layer model climate over western Europe and the frequency of occurrence of extreme values of temperture, precipitation and wind for selected grid boxes: the changes with 4 x CO_2 and prescribed sea surface temperatures. Met O 20 Tech Note II/224.

Figure Captions

Figure 1. Effect of using a discrete timestep.

(a) Cloud amount. Smooth dashed line, continuous variation; solid line, approximated every two hours; chain dotted line, approximated every six hours.

(b) Solar flux at the surface (Wm^{-2}). Solid line, cloud updated every two hours; chain dotted line, cloud updated every six hours.

Figure 2. Simulated total cloud cover for July. Contours every 0.2 cover, areas with greater than 0.5 cover shaded.

Figure 3. 10 day mean fields over North Africa from the control integration. Diurnal variation at points A, B and C shown in Figures 4 to 6 respectively.

(a) Absorption of solar radiation at the surface (contours every 25 Wm^{-2}).

(b) Mass divergence at $\sigma = 0.9$, sampled every 6 hours. The contour interval is 10^{-6} sec^{-1}, areas of convergence are shaded, and areas of convergence greater than 3×10^{-6} sec^{-1} are shaded heavily. The arrows indicate the strength and direction of the wind in the lowest layer of the model. (The

restricted area on this and some subsequent diagrams is because the data sampled more frequently than once a day is available at only a limited number of grid points).

(c) Total precipitation (contours every 2.5 mm/day, dashed contour at 1 mm/day and shaded where greater than 5.0 mm/day).

(d) Low cloud amount. Areas with greater than 0.5 cover shaded.

Figure 4. Diurnal variation at point A (25.5°N, 1.0°E) north of the North African rainband, averaged over 10 days in July. Solid line, control integration; dashed line, anomaly integration. Abscissa is time (GMT).

(a) Low cloud, (b) Convective cloud, (c) High cloud, (d) Surface temperature, (K), (e) Relative humidity in the lowest model layer (%), (f) Total precipitation (mm/day), (g) Absorption of solar radiation at the surface (Wm-2).

Figure 5. As 4, for point B (19.5°N, 0.0°W) on the northern edge of the rainband.

Figure 6. As 4, for point C (13.5°N, 0.3°W) in the centre of the rainband.

Figure 7. Day to day variation of globally averaged low cloud amount over land (fraction of total cover). Solid line, control integration, dashed line, anomaly integration.

Figure 8. Change in absorption of solar radiation at the surface due to increasing the interval between updating cloud amounts from 2 to 6 hours. Contours every 25 Wm^{-2} areas of decrease shaded. (July mean).

Figure 9. a-g as for Figure 4, but over North Africa (7.5°N to 34.5°N, 10°W to 35°E). (h) Specific humidity of the lowest model layer (g/kg), (i) Transfer of sensible heat from the surface (Wm^{-2}), (j) Medium cloud.

Figure 10. Changes over North Africa during a 10 day period in July due to increasing the interval between updating cloud amounts from 2 to 6 hours. Areas of decrease are shaded.

(a) Absorption of solar radiation at the surface (contours every 25 Wm^{-2}).

(b) Low cloud amounts (contours every 0.1 of total cover).

Figure 11. Changes in July mean fields due to increasing the interval between updating cloud amounts from 2 to 6 hours. (a) Precipitation (contours at 0, $\pm$ 1, $\pm$ 2 $\pm$ 5, $\pm$ 10 mm/day, areas of decrease shaded), (b) Total cloud (contours every 0.1 of total cover, areas of decrease shaded).

Figure 12. Changes in net downward radiation at the top of the atmosphere due to increasing the interval between updating cloud amounts from 2 to 6 hours. (Contours every 10 Wm^{-2}, areas of decrease are shaded).

Figure 13. a, b, c, as Figure 3a, b, c, but for the anomaly integration. Dashed line in Figure 13a 200 Wm^{-2} contour for control.

Figure 14. Changes in precipitation meaned over a 10 day period in July due to increasing the interval between updating cloud amounts from 2 to 6 hours. (Contours every 1 mm/day, areas of decrease are shaded).

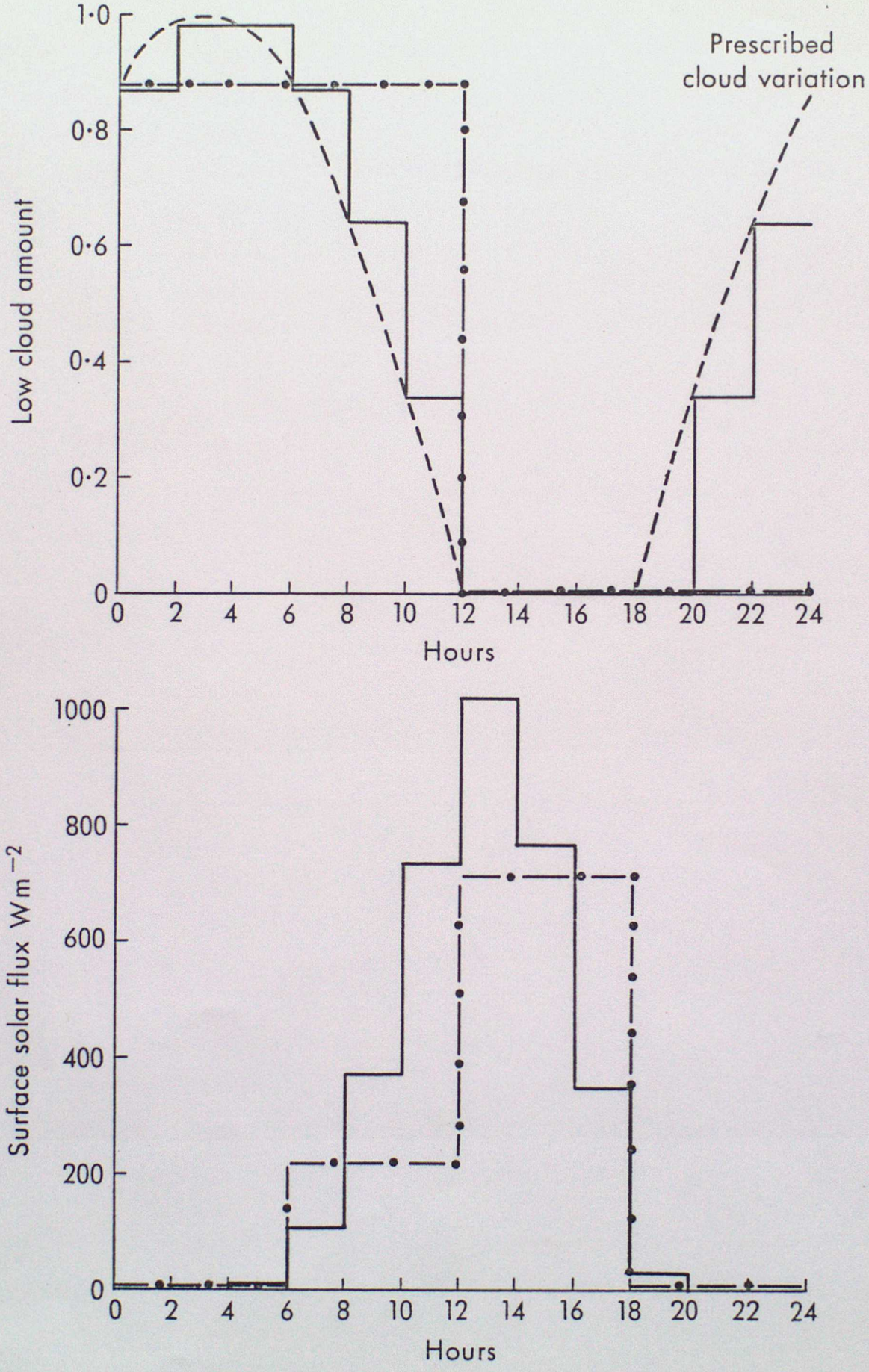
Prescribed
cloud variation
Low cloud amount
1·0
0·8
0·6
0·4
0·2
0
0 2 4 6 8 10 12 14 16 18 20 22 24
Hours
Surface solar flux Wm⁻²
1000
800
600
400
200
0
0 2 4 6 8 10 12 14 16 18 20 22 24
Hours

FIGURE 1

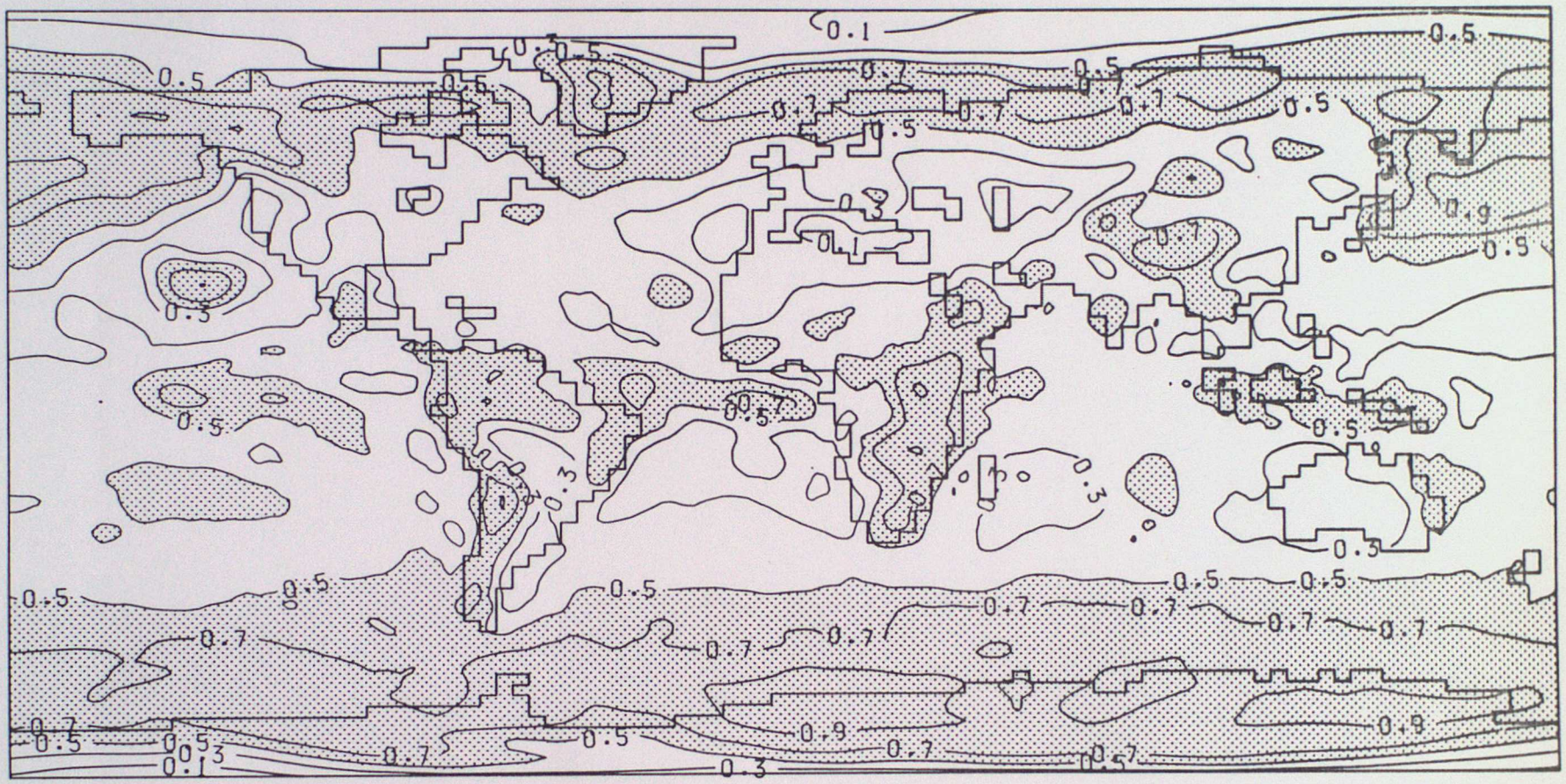

FIGURE 2

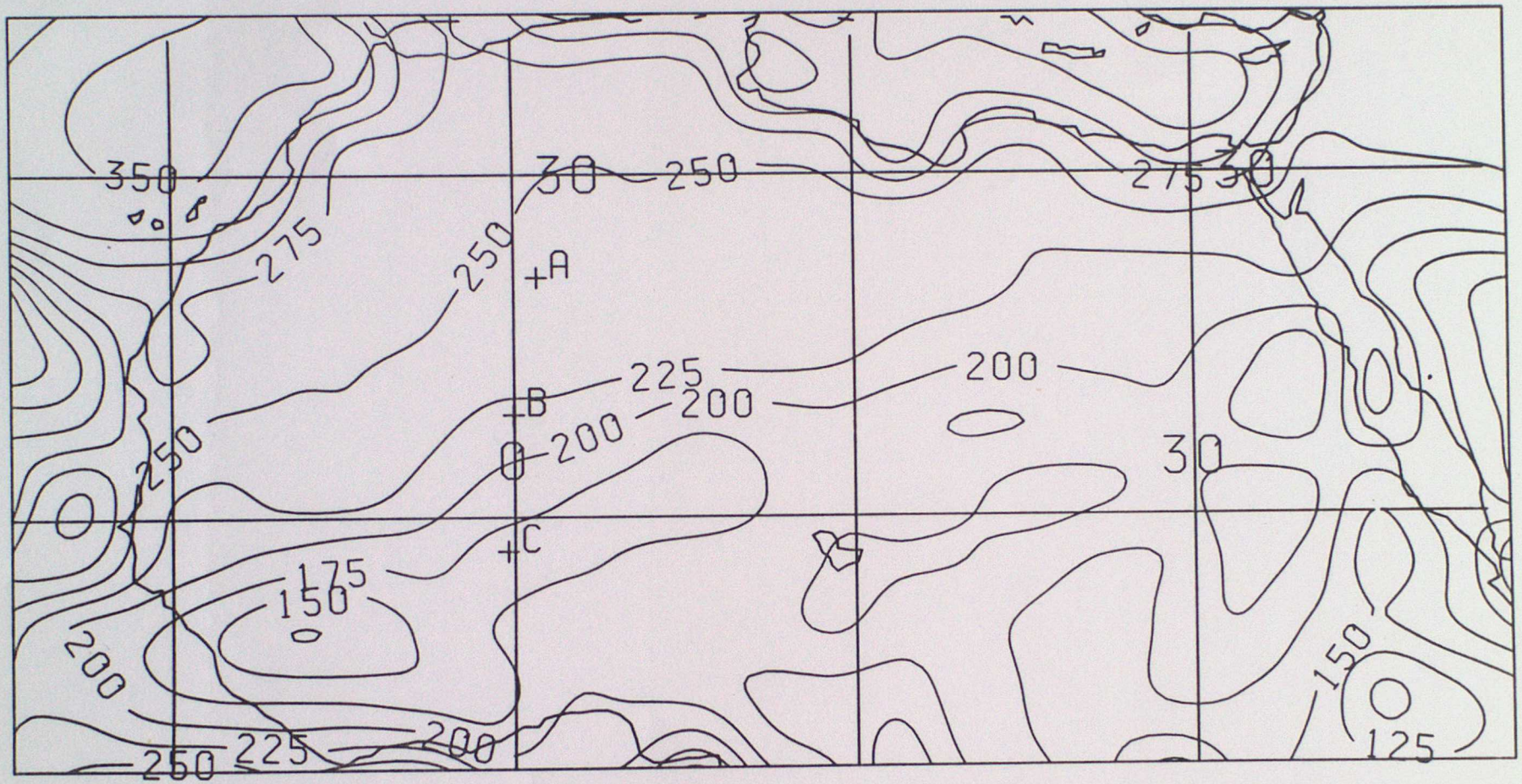
350
275
250
30
250
+A
225
200
B
200
200
250
C
175
150
200
250
225
200
275
30
30
150
125

FIGURE 3a

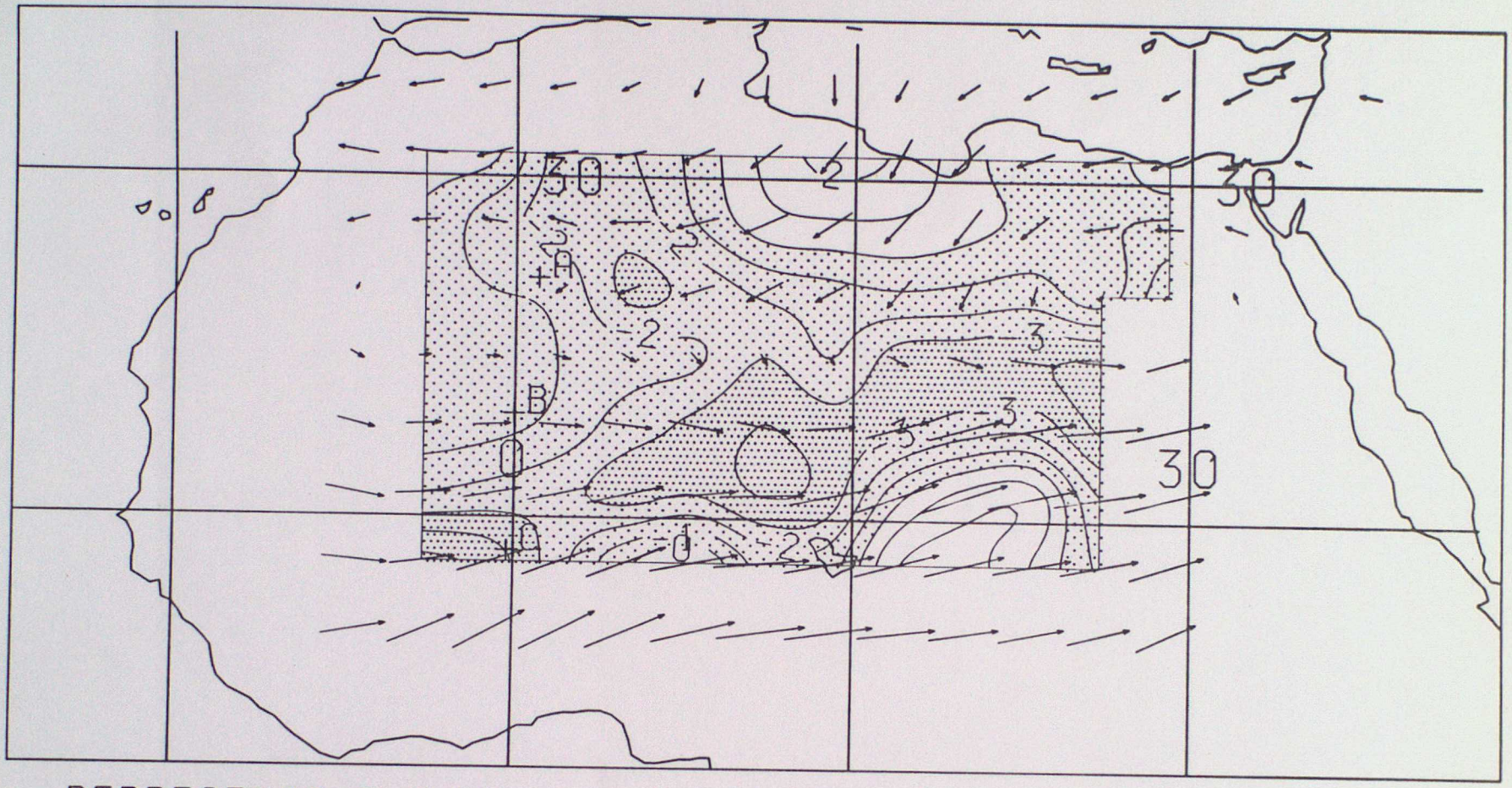

→ REPRESENTS 5 M/S

FIGURE 3b

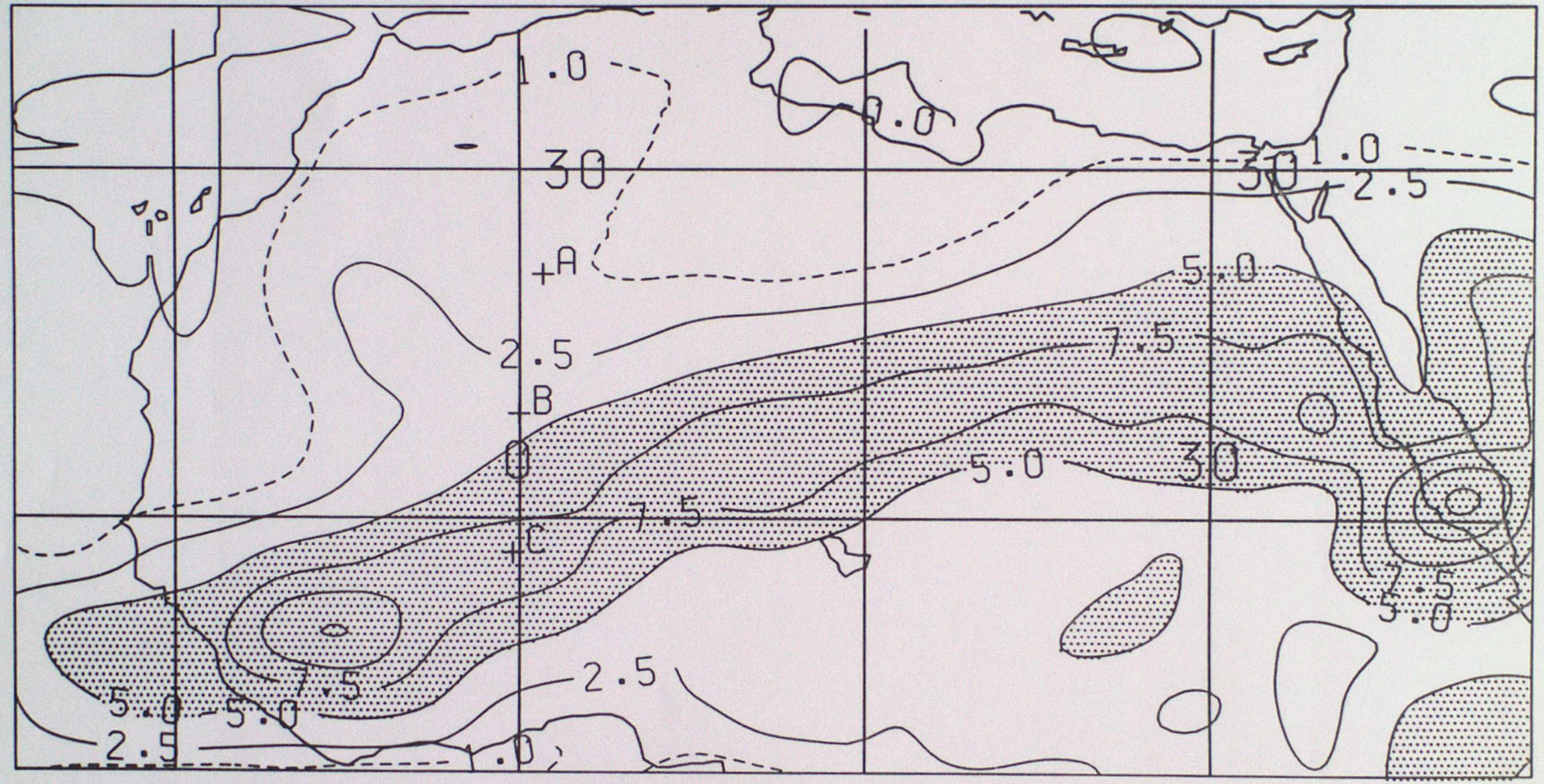

FIGURE 3c

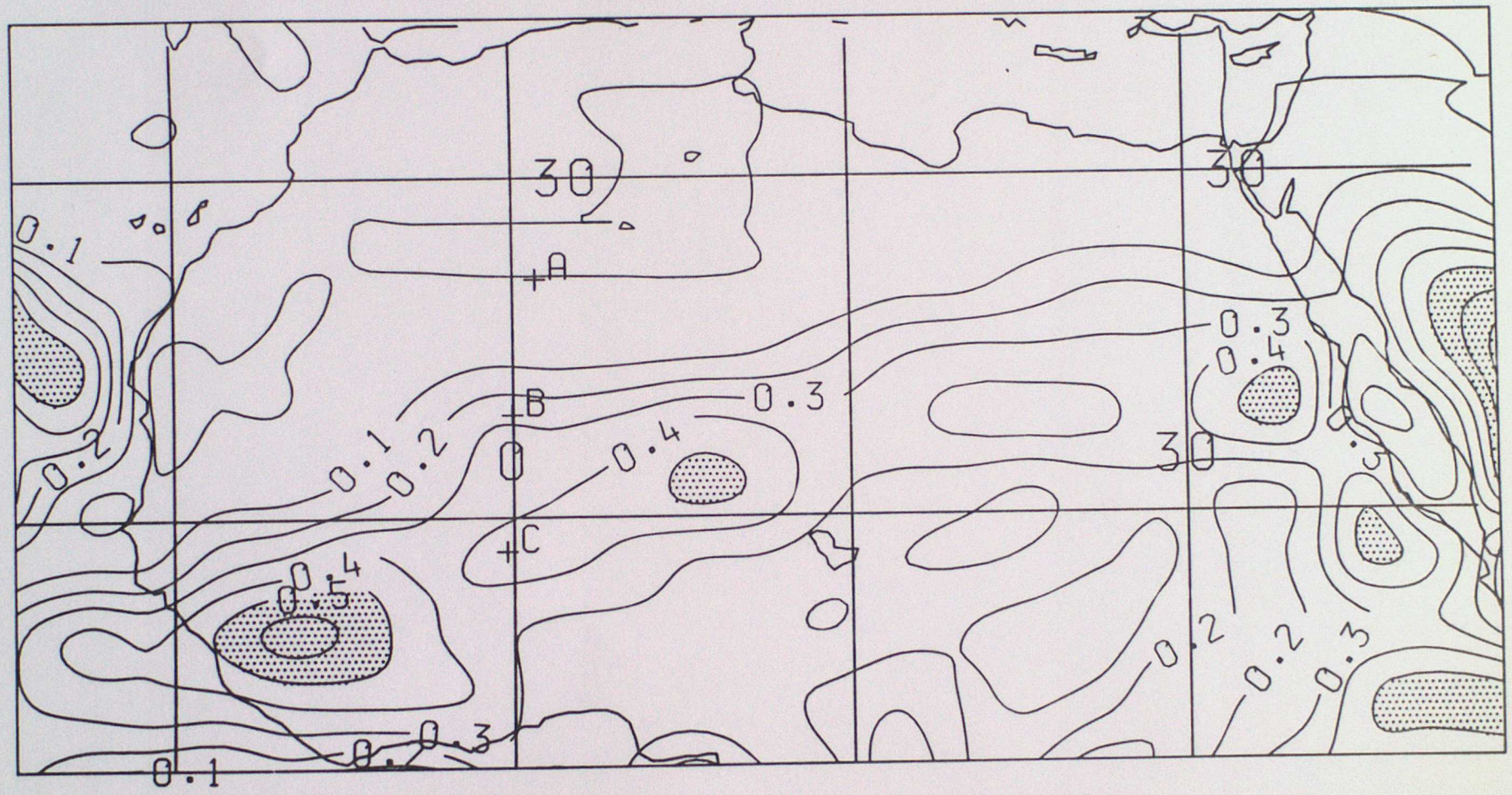

FIGURE 3d

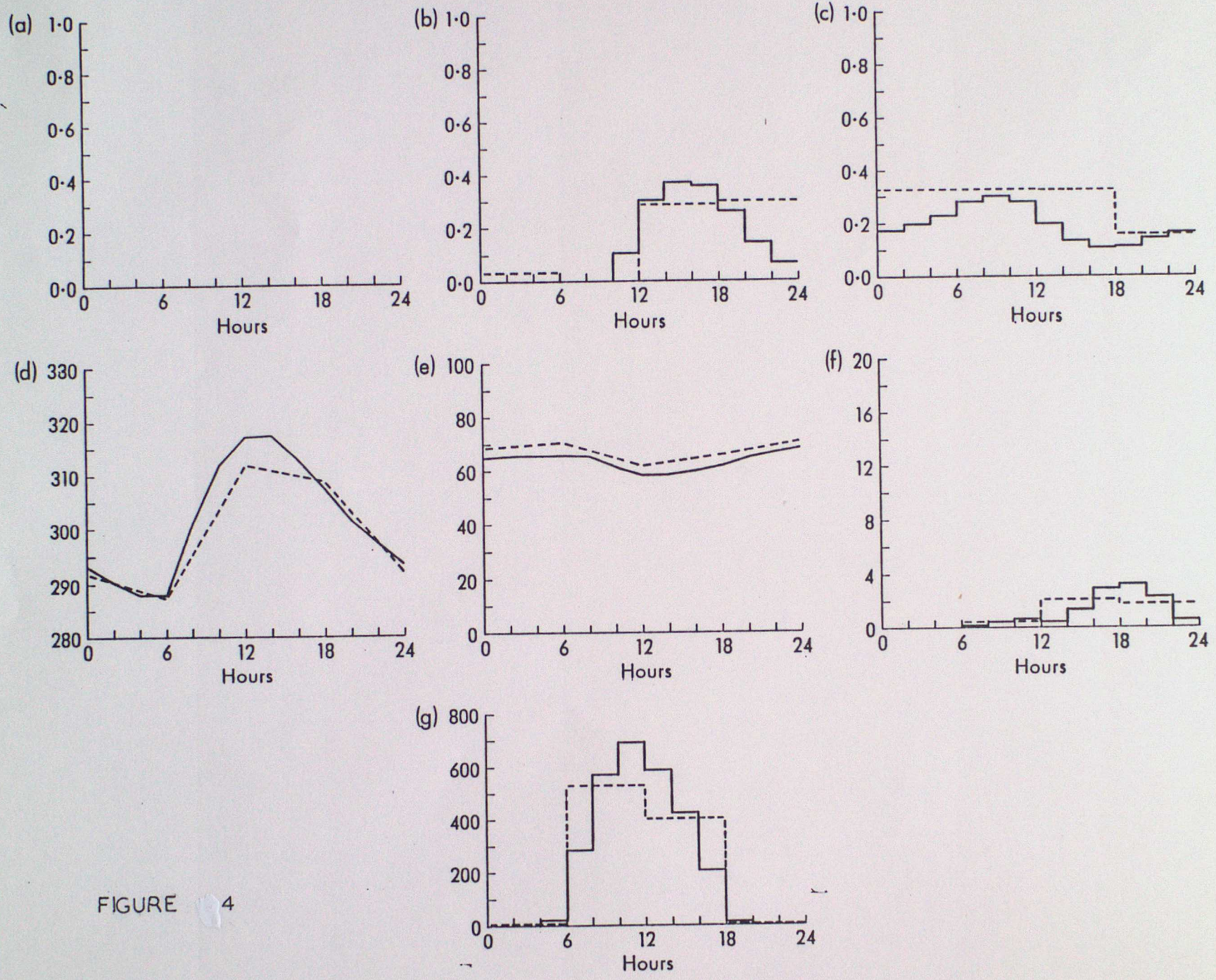
(a) 1·0
0·8
0·6
0·4
0·2
0·0
0
6
12
18
24
Hours
(b) 1·0
0·8
0·6
0·4
0·2
0·0
0
6
12
18
24
Hours
(c) 1·0
0·8
0·6
0·4
0·2
0·0
0
6
12
18
24
Hours
(d) 330
320
310
300
290
280
0
6
12
18
24
Hours
(e) 100
80
60
40
20
0
0
6
12
18
24
Hours
(f) 20
16
12
8
4
0
0
6
12
18
24
Hours
(g) 800
600
400
200
0
0
6
12
18
24
Hours

FIGURE 4

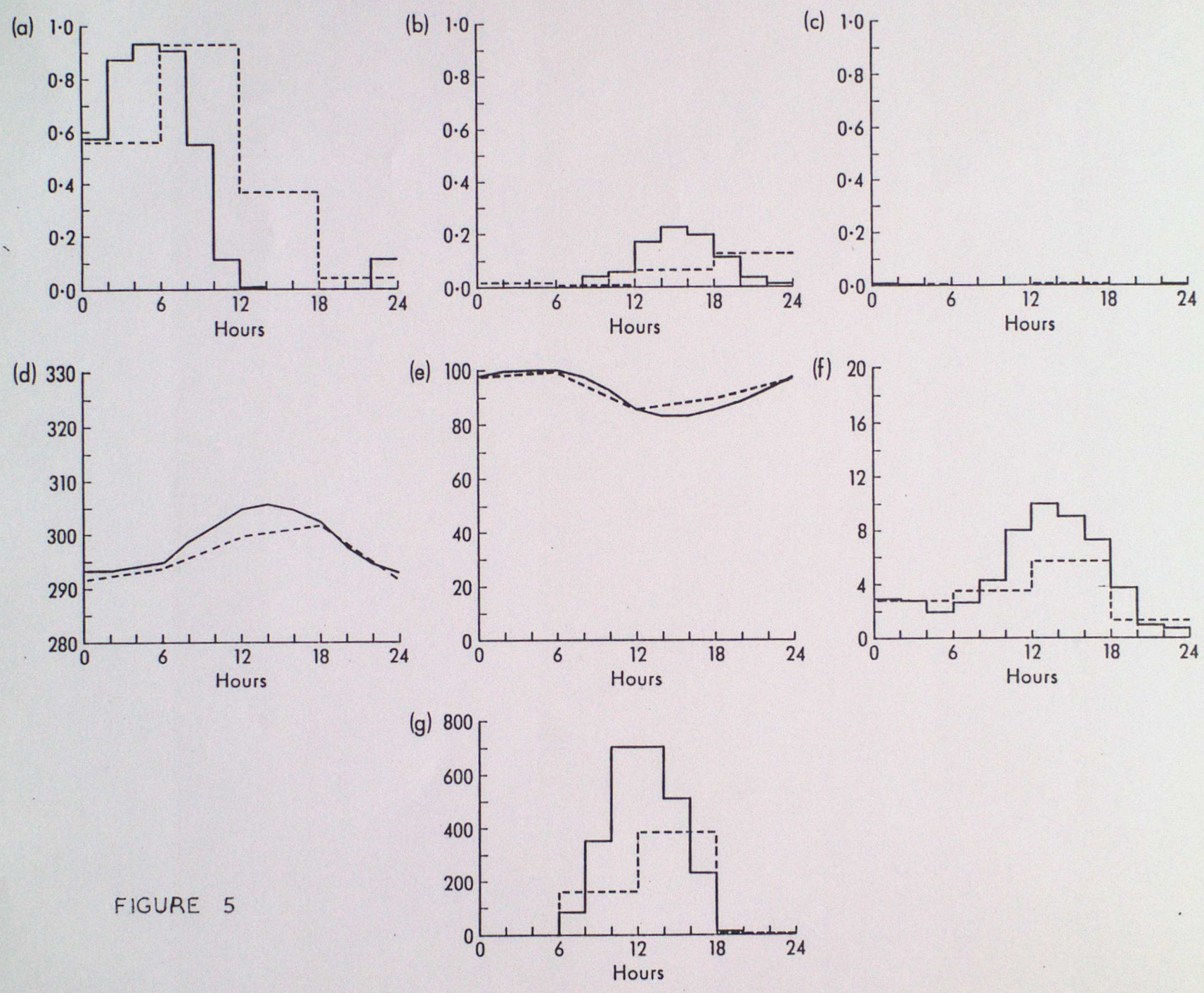
(a)
1·0
0·8
0·6
0·4
0·2
0·0
0
6
12
18
24
Hours
(b)
1·0
0·8
0·6
0·4
0·2
0·0
0
6
12
18
24
Hours
(c)
1·0
0·8
0·6
0·4
0·2
0·0
0
6
12
18
24
Hours
(d)
330
320
310
300
290
280
0
6
12
18
24
Hours
(e)
100
80
60
40
20
0
0
6
12
18
24
Hours
(f)
20
16
12
8
4
0
0
6
12
18
24
Hours
(g)
800
600
400
200
0
0
6
12
18
24
Hours

FIGURE 5

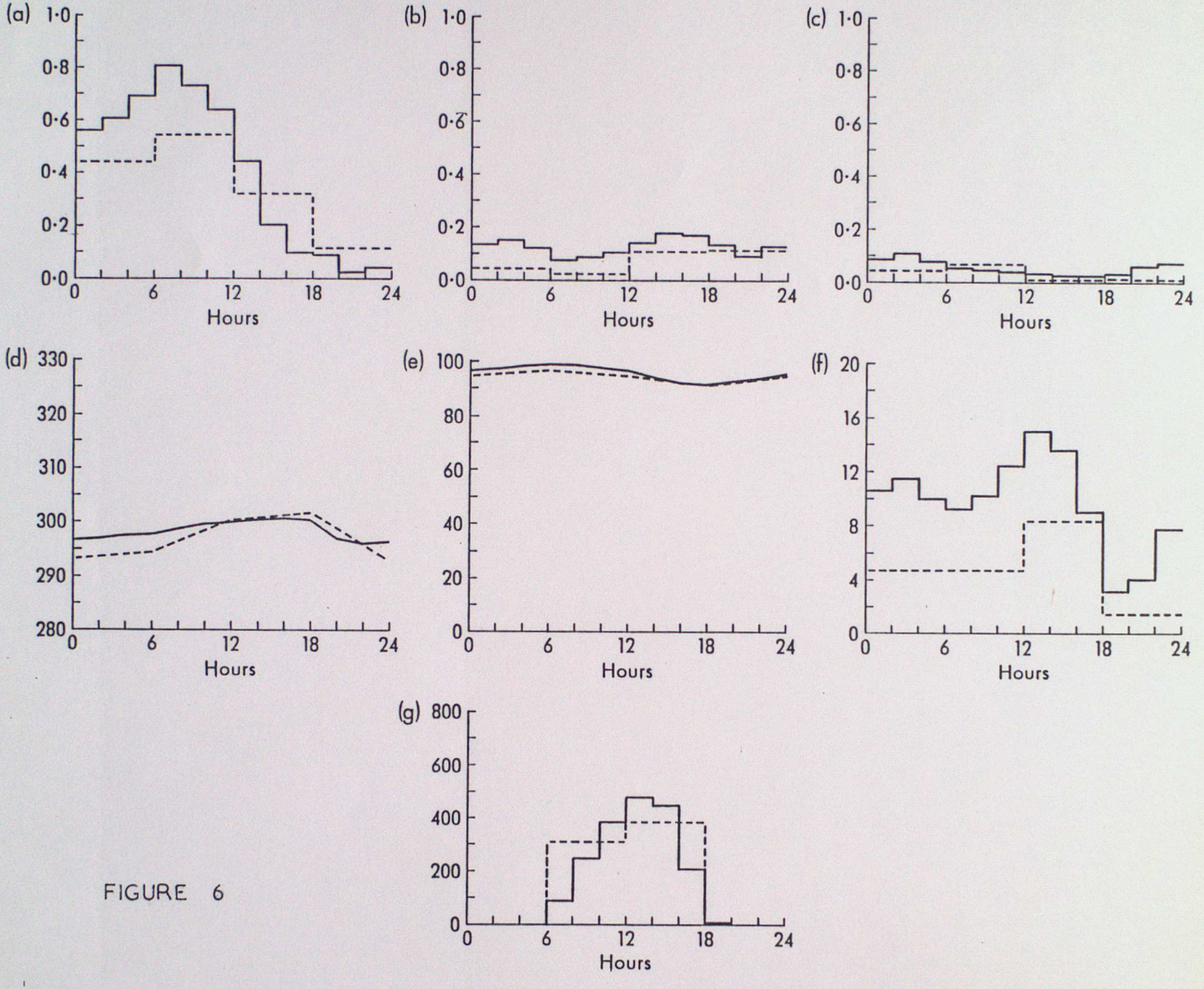
(a)
1·0
0·8
0·6
0·4
0·2
0·0
0
6
12
18
24
Hours
(b)
1·0
0·8
0·6
0·4
0·2
0·0
0
6
12
18
24
Hours
(c)
1·0
0·8
0·6
0·4
0·2
0·0
0
6
12
18
24
Hours
(d)
330
320
310
300
290
280
0
6
12
18
24
Hours
(e)
100
80
60
40
20
0
0
6
12
18
24
Hours
(f)
20
16
12
8
4
0
0
6
12
18
24
Hours
(g)
800
600
400
200
0
0
6
12
18
24
Hours

FIGURE 6

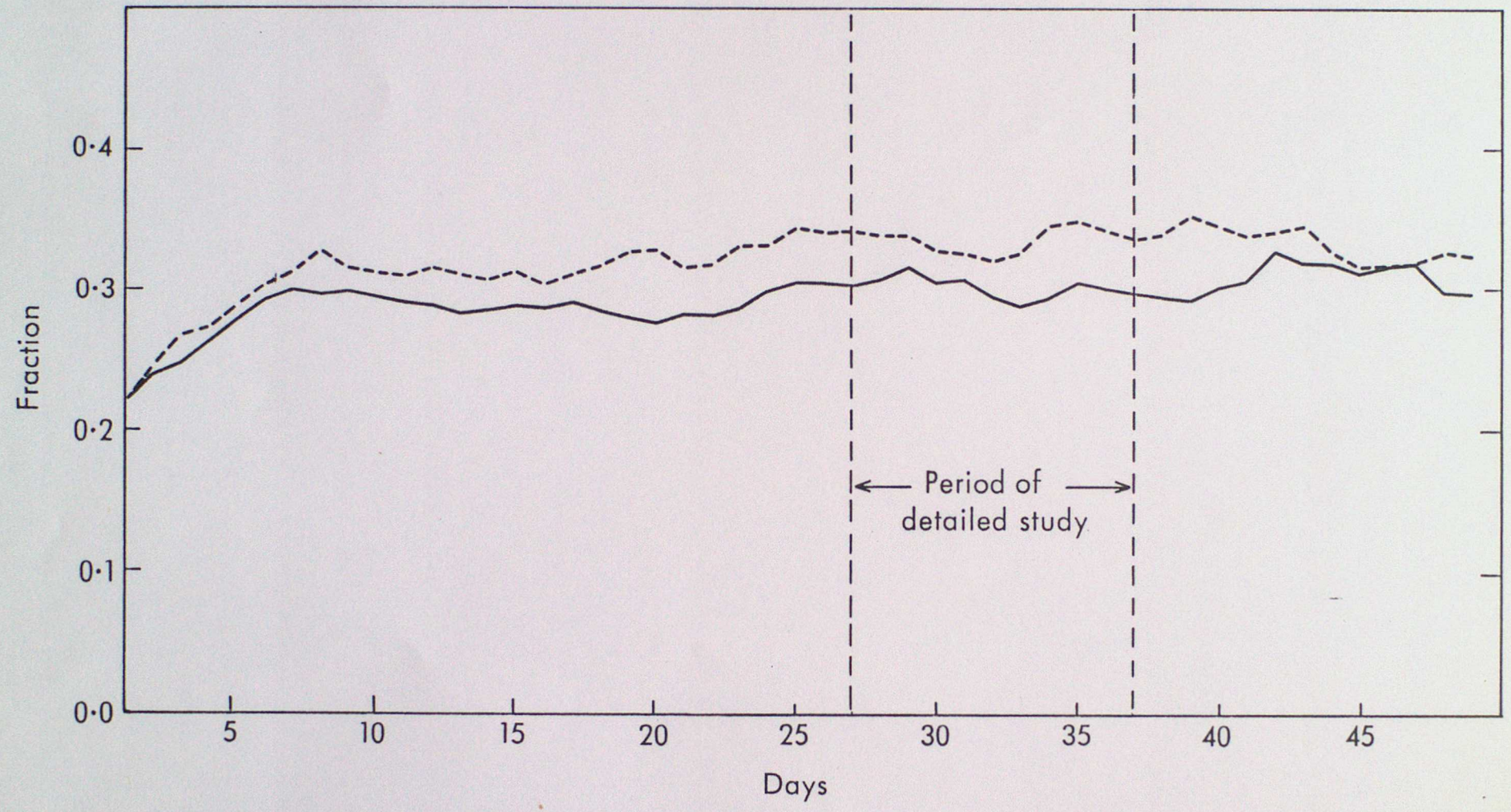
0·4
0·3
0·2
0·1
0·0
Fraction
5
10
15
20
25
30
35
40
45
Days
Period of
detailed study

FIGURE 7

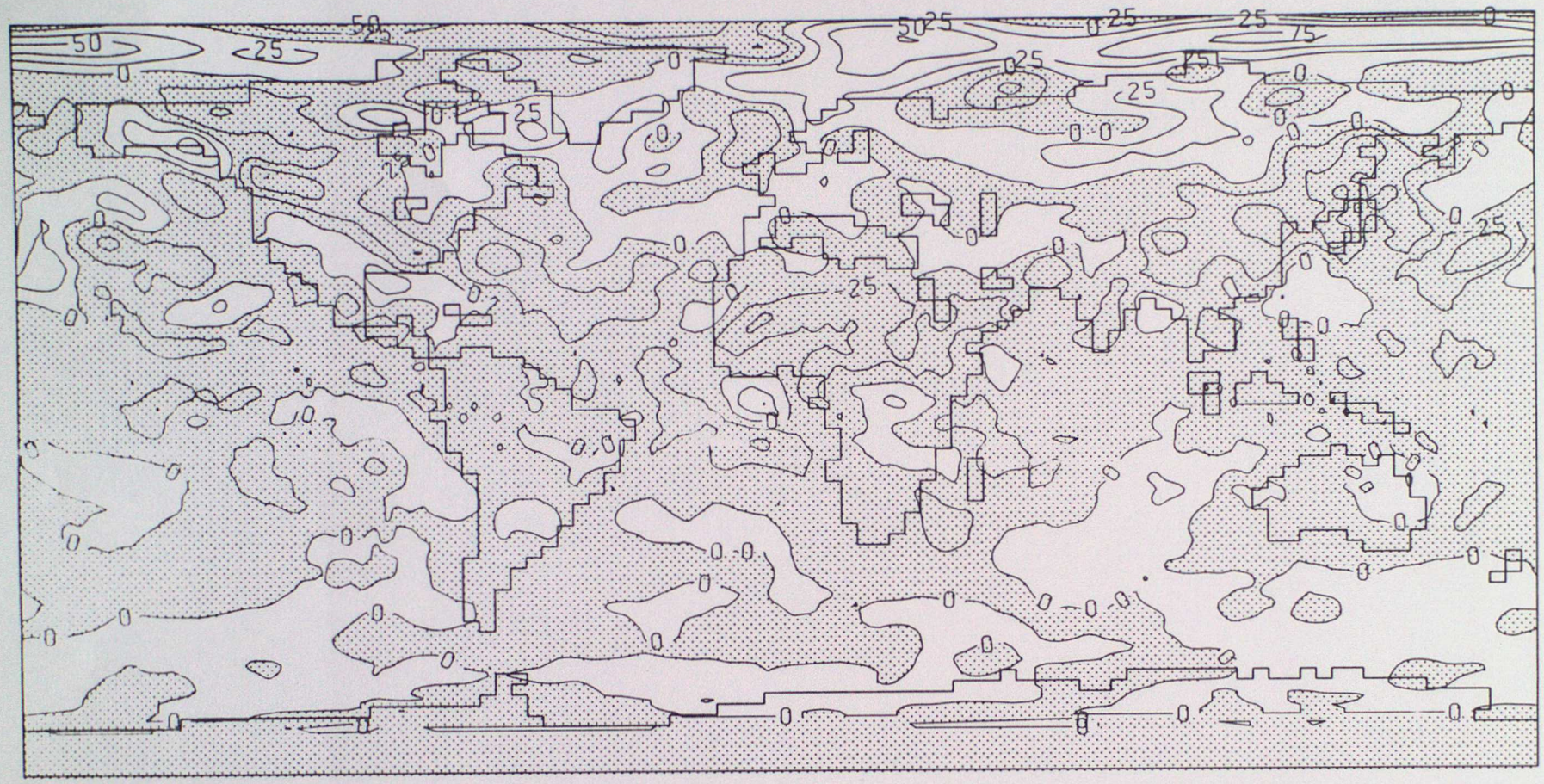

FIGURE 8

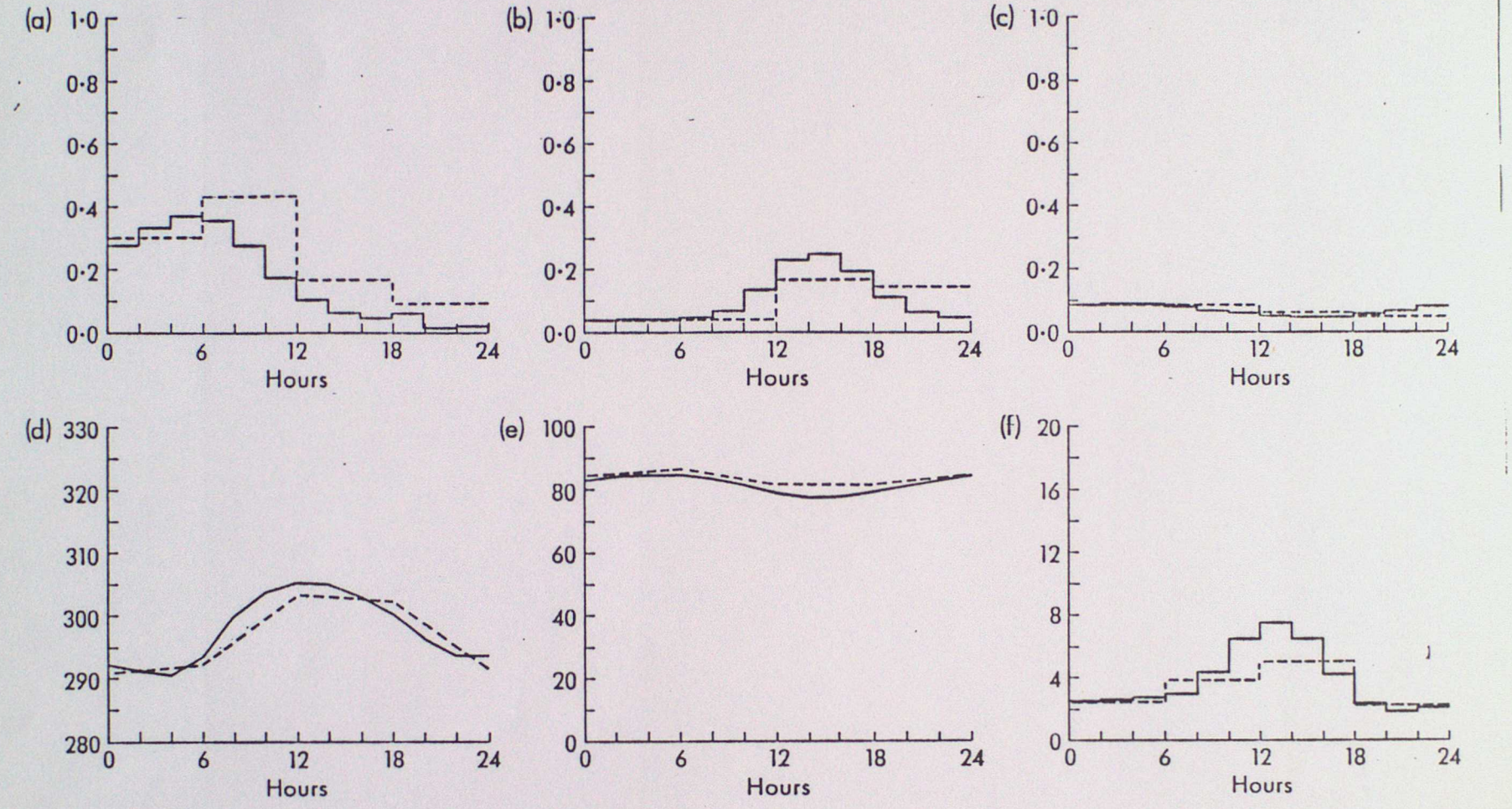
(a)
1·0
0·8
0·6
0·4
0·2
0·0
0
6
12
18
24
Hours
(b)
1·0
0·8
0·6
0·4
0·2
0·0
0
6
12
18
24
Hours
(c)
1·0
0·8
0·6
0·4
0·2
0·0
0
6
12
18
24
Hours
(d)
330
320
310
300
290
280
0
6
12
18
24
Hours
(e)
100
80
60
40
20
0
0
6
12
18
24
Hours
(f)
20
16
12
8
4
0
0
6
12
18
24
Hours

FIGURE 9

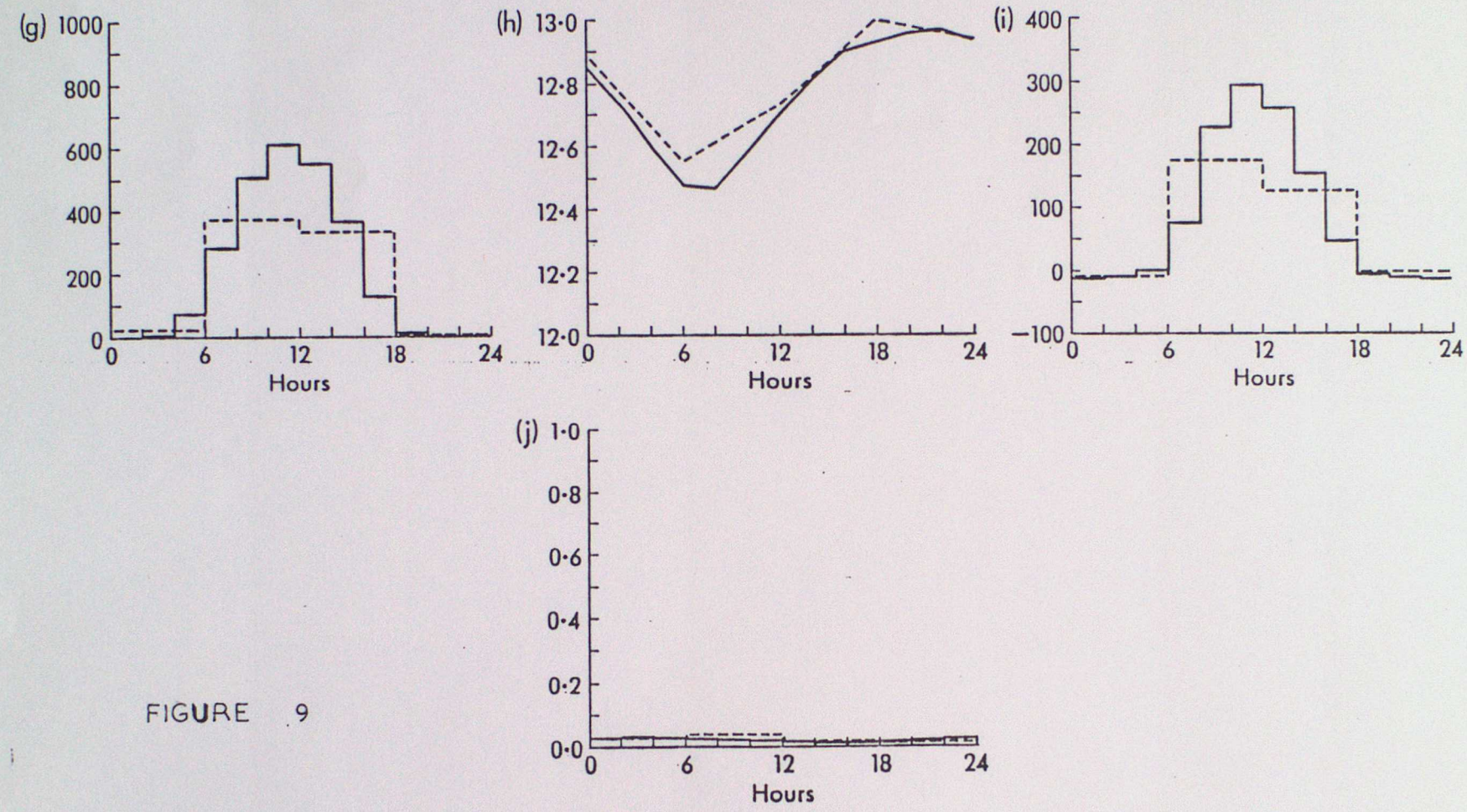
(g) 1000
800
600
400
200
0
0
6
12
18
24
Hours
(h) 13·0
12·8
12·6
12·4
12·2
12·0
0
6
12
18
24
Hours
(i) 400
300
200
100
0
−100
0
6
12
18
24
Hours
(j) 1·0
0·8
0·6
0·4
0·2
0·0
0
6
12
18
24
Hours

FIGURE 9

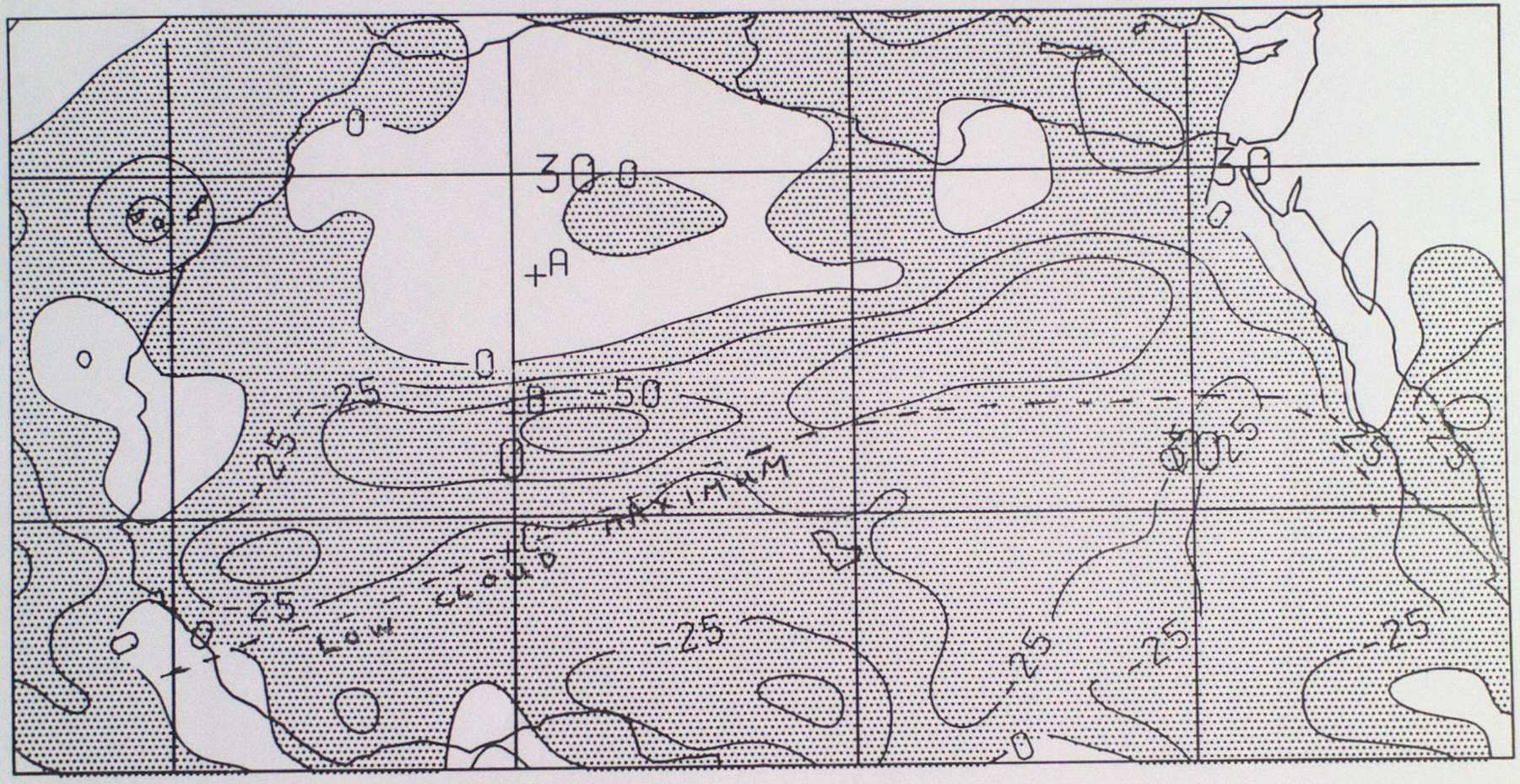

FIGURE 10a

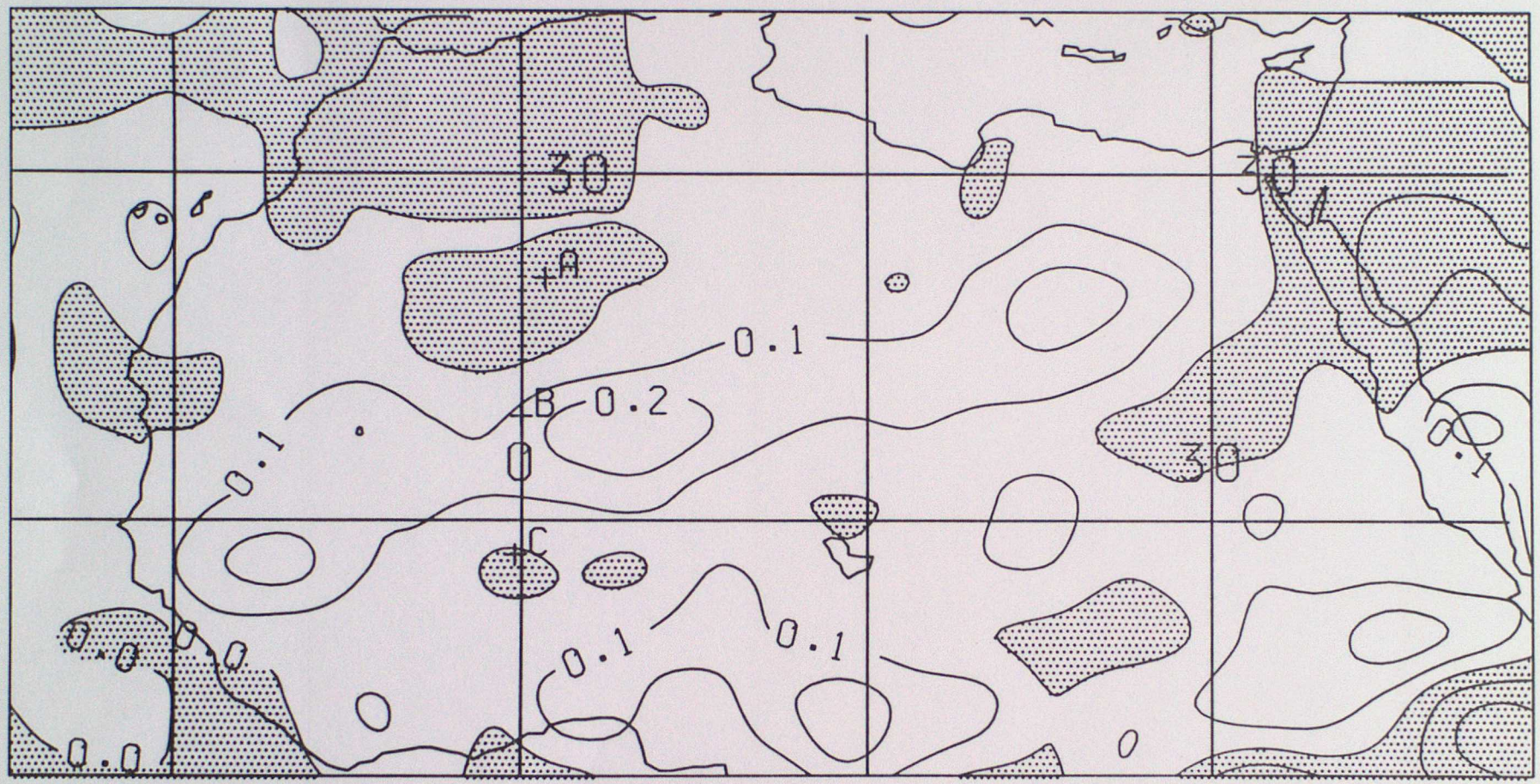

FIGURE 10b

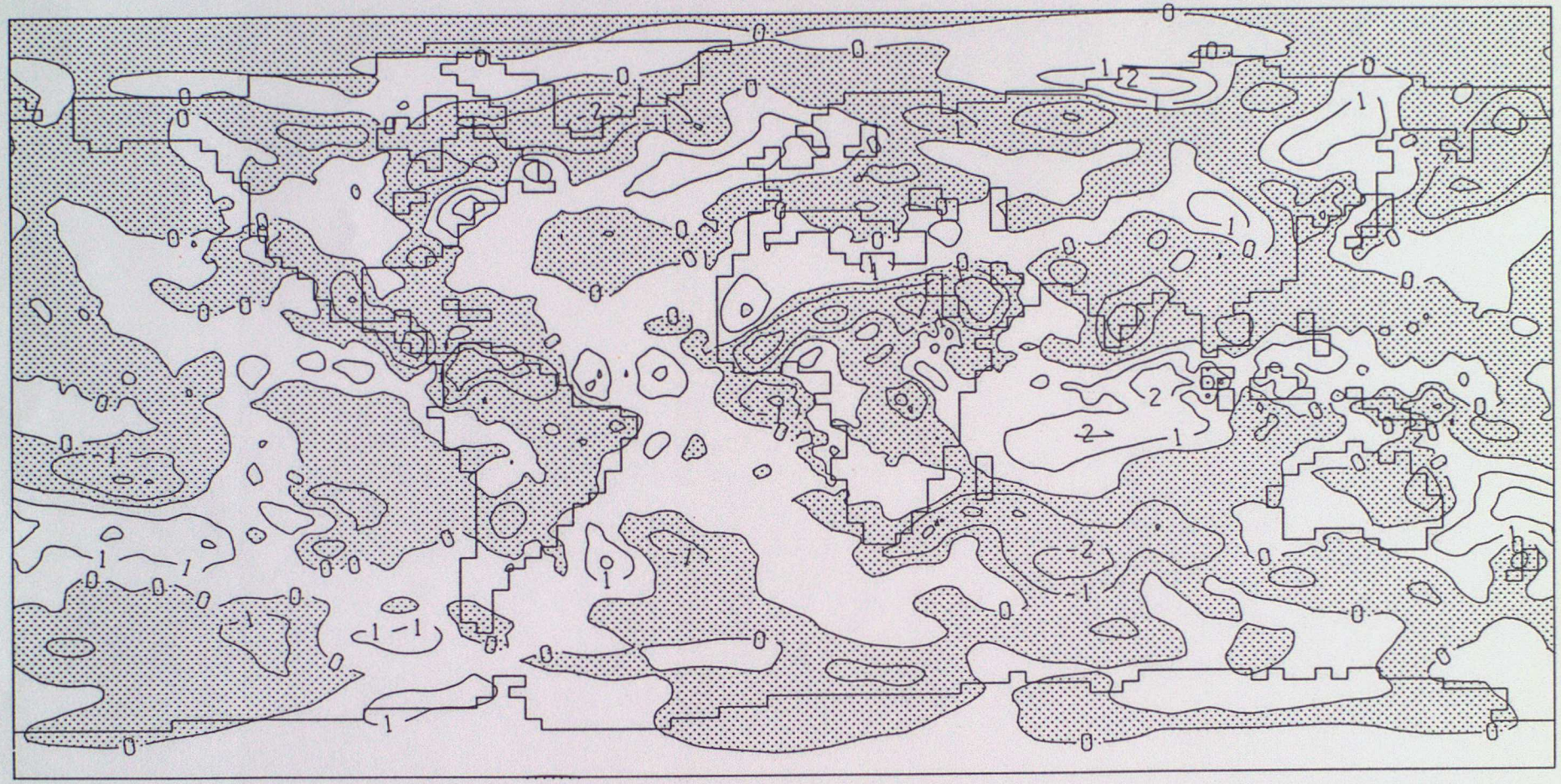

FIGURE 11a

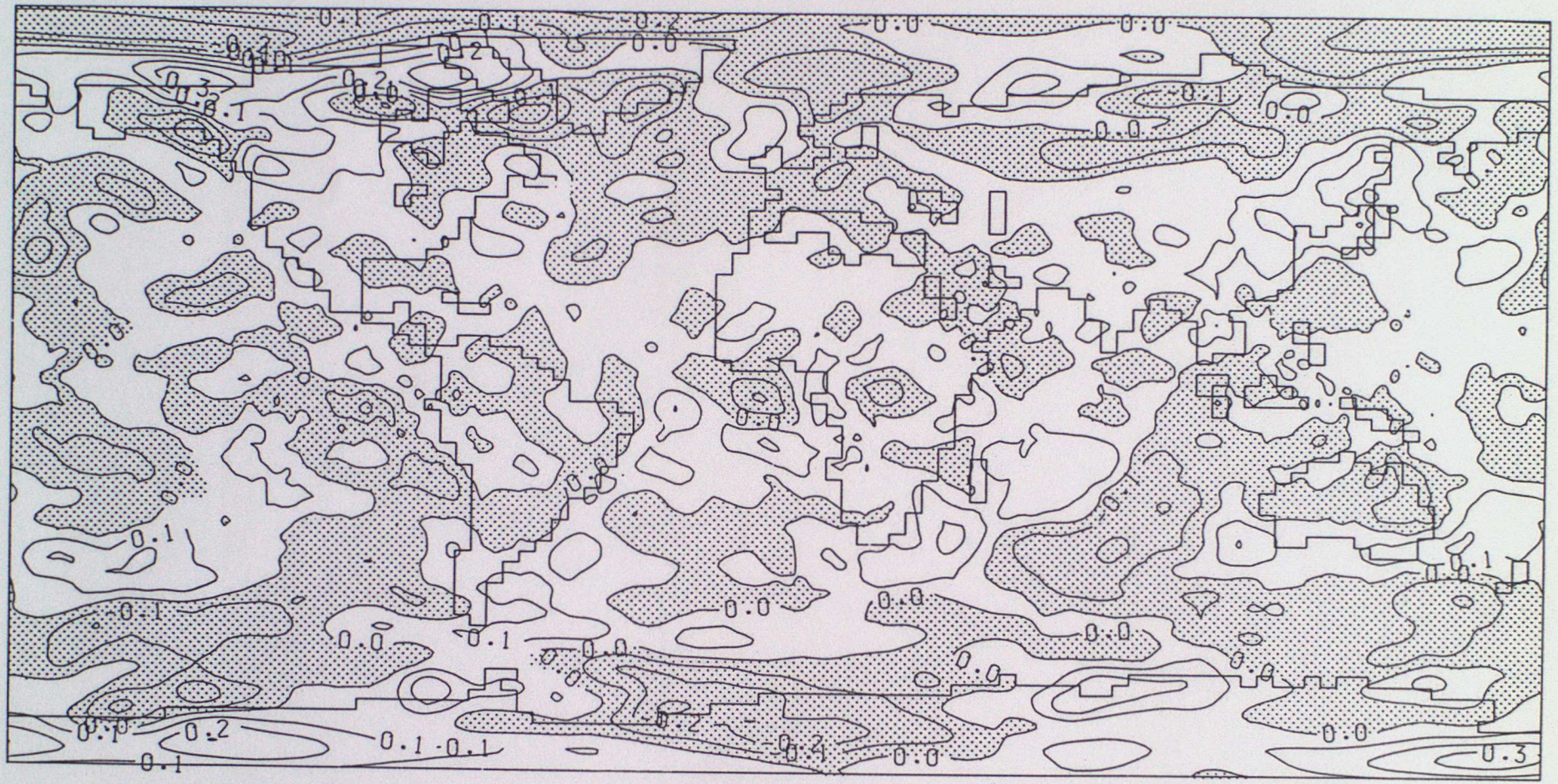

FIGURE 11b

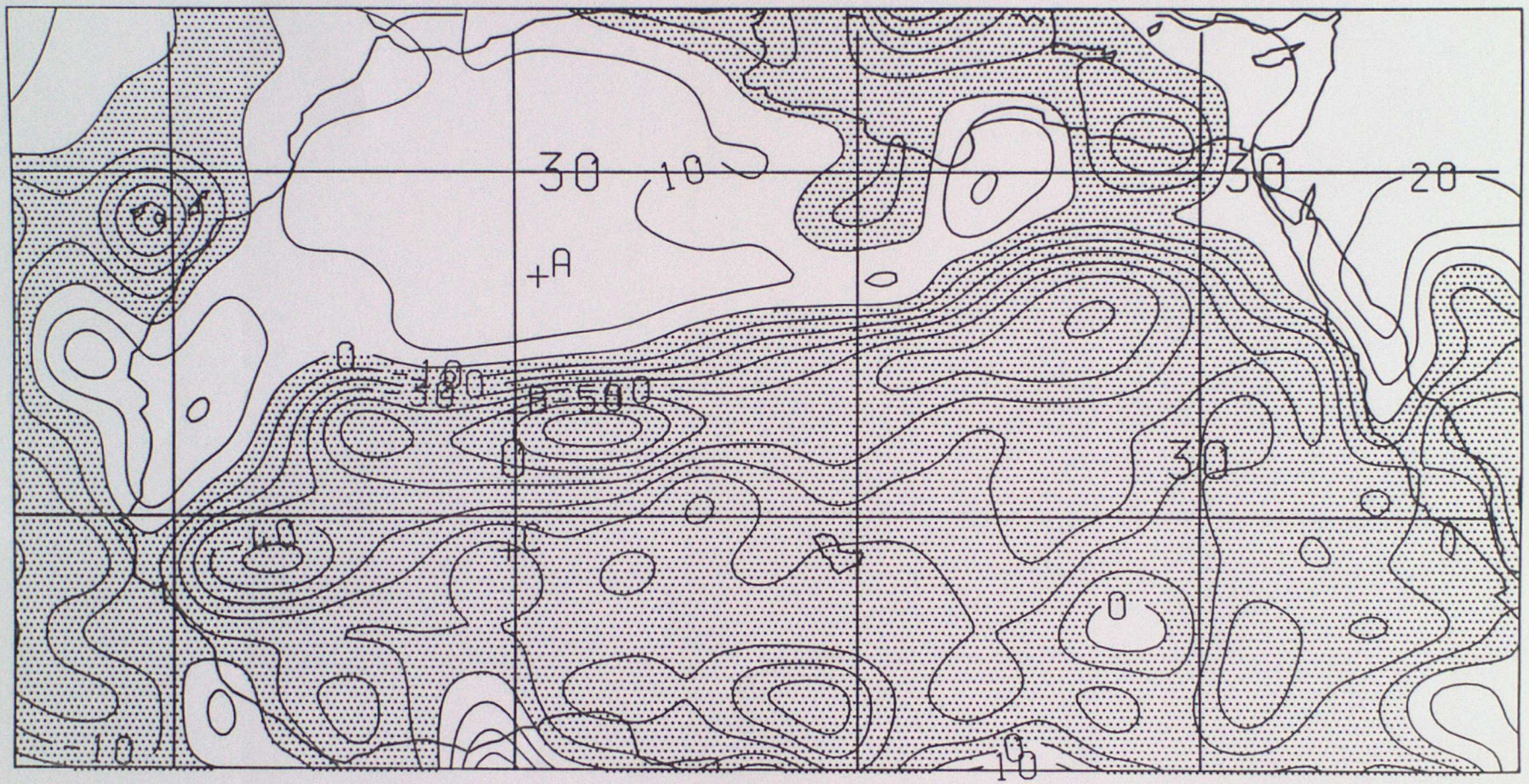

FIGURE 12

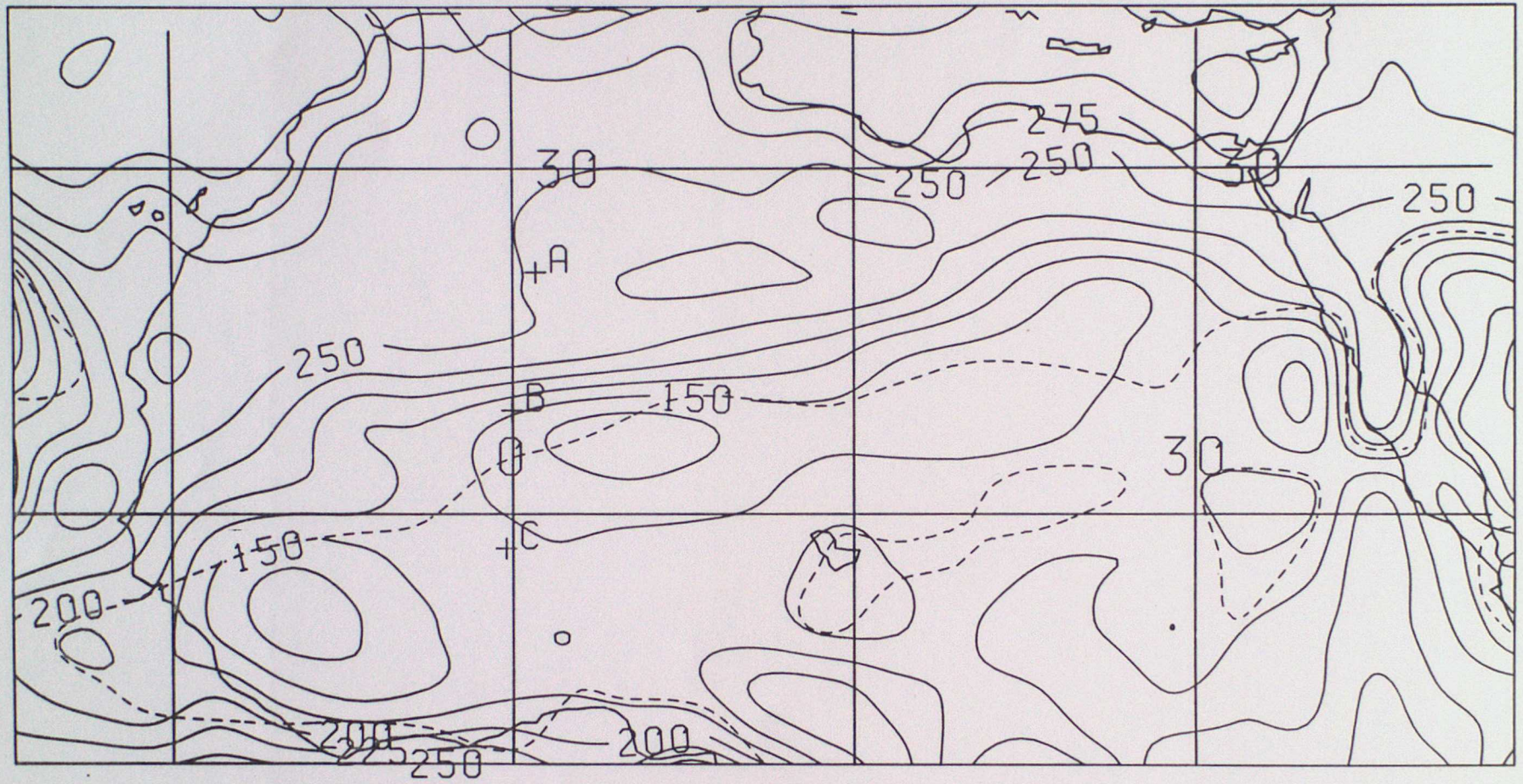

FIGURE 13a

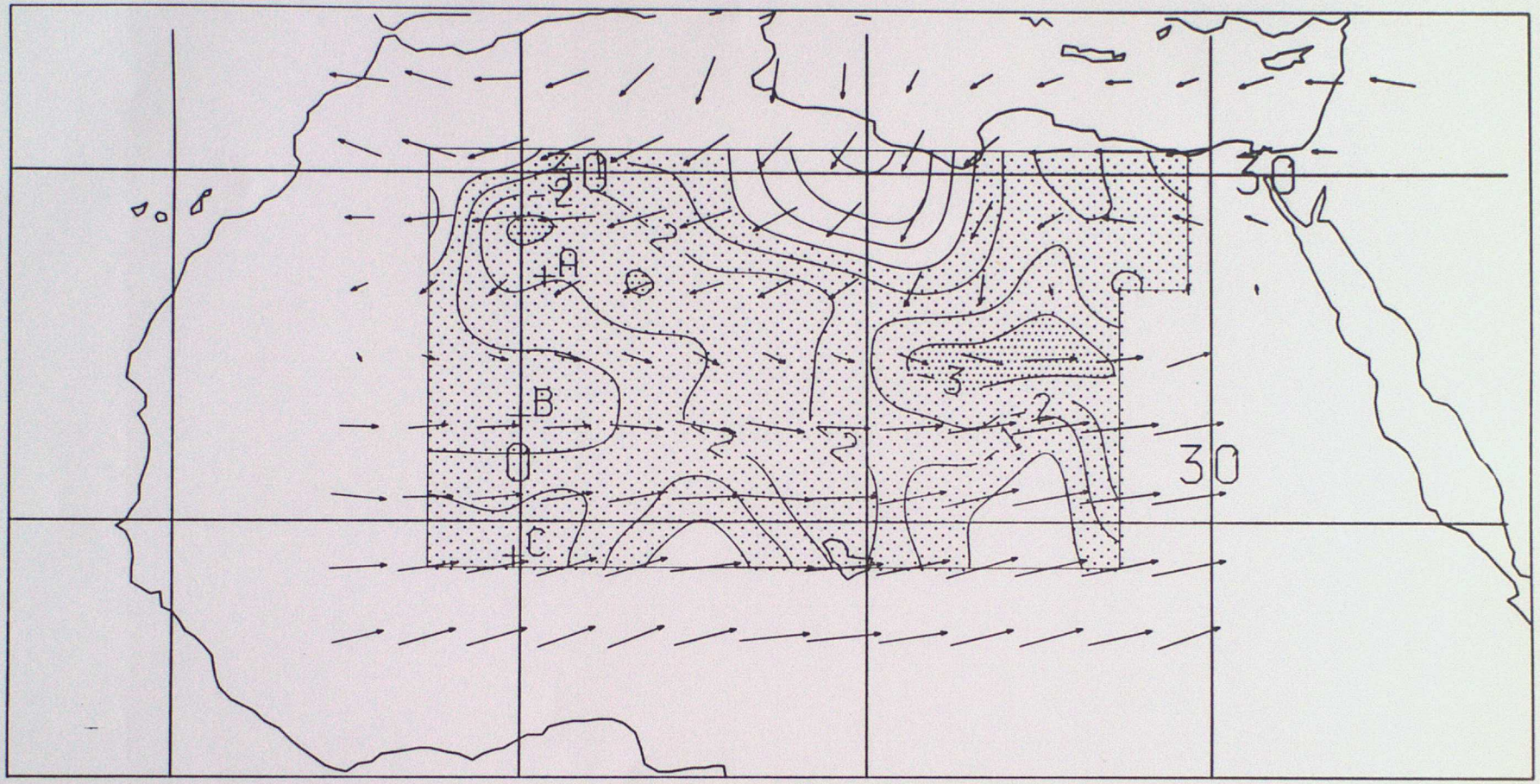

→ REPRESENTS 5 M/S

FIGURE 13b

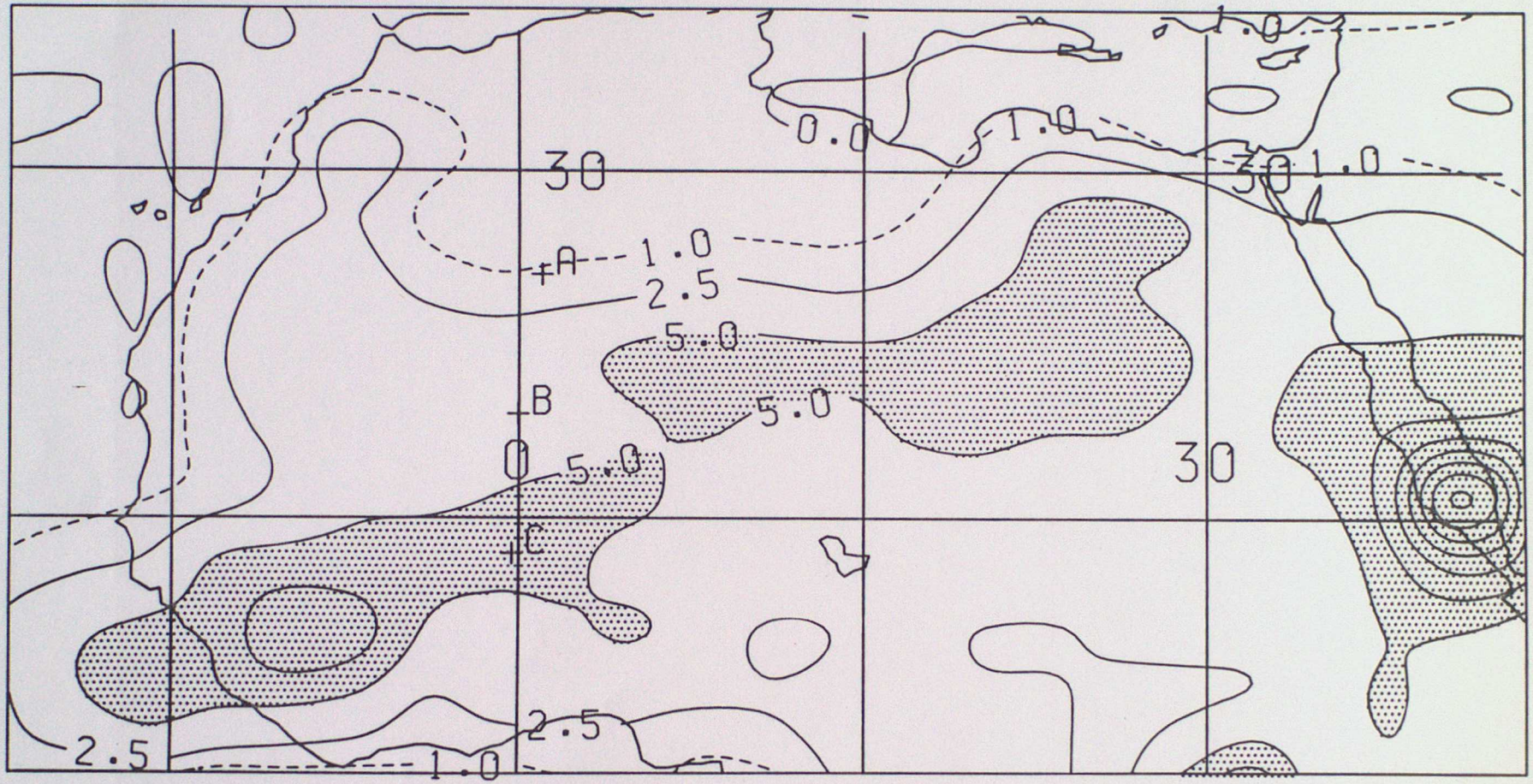

FIGURE 13c

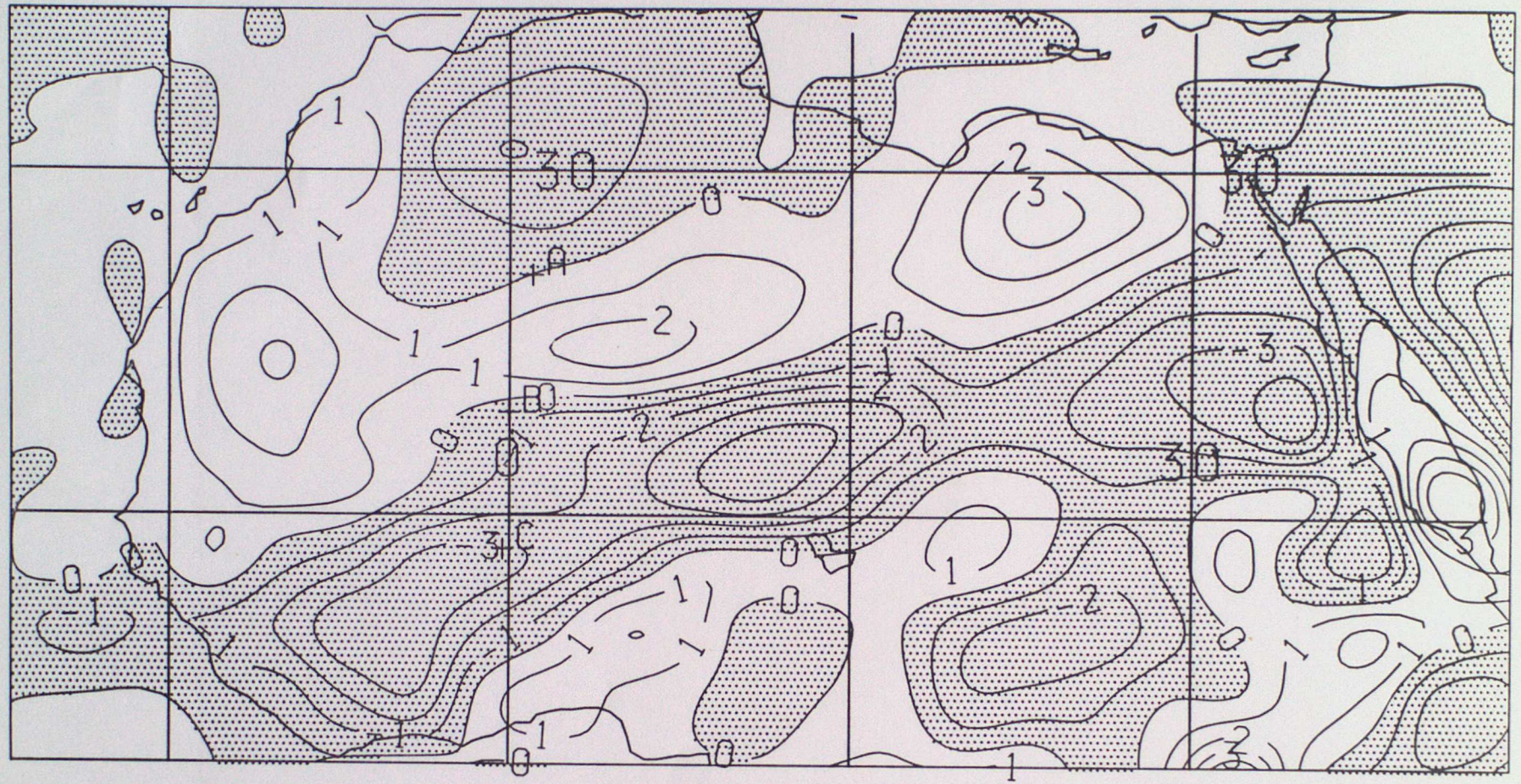

FIGURE 14